Aus dem Institut für Neuropathologie
der Heinrich-Heine-Universität Düsseldorf
Direktor: Univ.-Prof. Dr. med. Guido Reifenberger

Molecular and functional analysis of *SOCS3* in human glioblastomas

Dissertation

zur Erlangung des Grades eines Doktors der Medizin
der Medizinischen Fakultät der Heinrich-Heine-Universität Düsseldorf

vorgelegt von
Carina Lindemann
2012

Als Inauguraldissertation gedruckt mit der Genehmigung der Medizinischen Fakultät der Heinrich-Heine-Universität Düsseldorf:

gez.:

Dekan: Univ.-Prof. Dr. med. Joachim Windolf

Referent: Univ.-Prof. Dr. med. Markus Johannes Riemenschneider

Korreferent: Univ.-Prof. Dr. med. Rainer Haas

Teile dieser Arbeit wurden veröffentlicht:

Lindemann C, Hackmann O, Delic S, Schmidt N, Reifenberger G and Riemenschneider M. J (2011) *SOCS3* promoter methylation is mutually exclusive to *EGFR* amplification in gliomas and promotes glioma cell invasion through STAT3 and FAK activation. Acta Neuropathol 122:241-51.

Table of Contents

1 Introduction

Tumors of the central nervous system represent approximately 2-3 % of all cancers diagnosed in the Western world and therefore belong to the more rarely occurring tumors (Westphal et al. 2003). The prevalence has been estimated to 69 patients/ 100 000 population and the incidence is around 15 new cases/ 100 000 inhabitants per year (Ohgaki et al. 2005). The percentage of brain tumors among all cancers is higher in children than in adults. Here, they represent the second most commonly diagnosed neoplasms after the group of leukemias (Bondy et al. 2008).

1.1 Overview and epidemiology of glioblastomas

Gliomas are the most common primary tumors of the central nervous system (around 50 %) and they comprise a heterogeneous group of neoplasms composed of neoplastically transformed glial cells (Louis et al. 2007).
Gliomas are histologically classified according to the WHO (World Health Organisation) classification of tumors of the central nervous system in its latest edition from 2007 (first edition: 1956 and 1957). The WHO classification separates primary brain tumors into different histological subtypes and assigns a specific WHO malignancy grade to each tumor, ranging from WHO grade I (benign) to WHO grade IV (highly malignant). However, genetic alterations become more and more important with respect to brain tumor classification into prognostically distinct subgroups (Riemenschneider et al. 2010).
Tumor classification and grading helps in finding suitable therapeutic strategies and constitute an important predictor of prognosis. Individual tumor types "prefer" a certain age: while pilocytic astrocytomas mainly occur in childhood and young age (< 20 years), diffuse and anaplastic astrocytomas and oligodenroglial tumors of the cerebral hemispheres are mostly found in middle aged patients (30 - 50 years), while glioblastomas are most common in patients older 50 years of age (Kleihues et al. 2003).

Glioblastomas (WHO grade IV) represent the most common and - at the same time - the most malignant primary brain tumors. These tumors represent 15-20 % of all intracranial tumors

and almost 50 % of all glial tumors (Kleihues et al. 2003). Glioblastomas or other diffusely infiltrative gliomas are growing very fast and infiltrate healthy surrounding brain parenchyma, which is a major reason why they cannot be completely removed by surgical resection. Despite many new multimodal therapy concepts (resection with subsequent radio- and chemotherapy) and intensive basic research efforts, the prognosis of glioblastoma is still unfavorable. The course of disease is usually rapidly progressive and the mean overall-survival (with a few exceptions with longer survival) is only about 12-15 months after diagnosis (Ohgaki and Kleihues 2007).
Glioblastomas can divided into two groups depending on their clinical history. Primary glioblastomas arise *de novo* (95 %) with no proof of less malignant precursor lesion whereas secondary glioblastomas originate through progression from pre-existing low-grade or anaplastic astrocytomas (5 %, Ohgaki et al. 2005).

These facts and the poor prognosis of glioblastoma patients clearly indicate that more research is needed to better understand their pathogenesis and to develop new and individualized therapeutic strategies.

1.1.1 Age and gender distribution

Glioblastomas preferentially affect adults with a peak incidence between 45 – 70 years, but may manifest at any age. Males are slightly more often affected than females (male: female 1.35:1; Kleihues et al. 2003).

1.1.2 Localization

Glioblastomas mostly develop in the cerebral hemispheres. Tumor invasion often spreads into the contralateral hemisphere and can also affect the basal ganglia. Children are more frequently diagnosed with glioblastomas of the brainstem (8.8 % of total glioblastoma patients, 3.3 % brainstem localization; Schiffer et al. 1976).

1.1.3 Etiology

The etiology of glioblastoma mostly remains unknown. Less than 1 % of all glioblastomas are associated with a genetic syndrome caused by inherited rare mutations (e.g. Turcot syndrome or Li-Fraumeni syndrome; Farrell et al. 2007). Whether the use of mobile phones could increase the risk for the development of glioblastomas is controversial (Lönn et al. 2005, Lahkola et al. 2007).

1.1.4 Symptoms

The clinical symptoms of glioblastoma patients depend on the area of the central nervous system that is affected by tumor growth. Glioblastomas of the cerebral hemispheres often cause non-specific neurological symptoms i.e. nausea, vomiting and headaches, or seizures and cranial nerve disorders as a result of a rapid development of increased intracranial pressure (increasing cerebral oedema). A glioblastoma located next to the optic nerve can cause visual loss. Other symptoms e.g. personality changes (due to location in the frontotemporal hemispheres) or spastic paresis, pain or extremities numbness (increased compression) are other possible symptoms (Kleihues et al. 2003).
Rare case reports indicate glioblastoma dissemination via the blood or the cerebrospinal fluid, with metastases being preferentially located in regional lymph nodes, pleura and lung, liver and bone (Frappaz et al. 1999; Pasquier et al. 1980). In general, however, metastasis formation is highly uncommon.

1.1.5 Diagnosis and therapy

Patients presenting with newly developed neurological symptoms are nowadays usually subjected to neuroimaging. On MRI, glioblastomas mostly present as intraaxial space-occupying lesions, often as a marginally contrast-enhancement ring structure that corresponds to the highly vascularized peripheral area of the tumor, and a central hypointense area corresponding to necrotic tumor parts. This ring structure does not denote the outer neoplasm borders, which could be proven in biopsy analyses and autoptic brain sections. Glioblastoma cells normally infiltrate diffusely in the surrounding non-neoplastic brain tissue up to 2 cm or more. T2-weighted MRI images are of limited value for measuring the tumor extension,

because the ‘tumor zone’ often overlaps with surrounding oedema (Dean et al. 1990, Kieffer et al. 1982). On CT scans with contrast medium, glioblastomas typically present as irregularly formed lesions with peripheral ring enhancement surrounding a hypodense central area of necrosis (Latchaw et al. 1991). Glucose consumption in positron emission tomography (PET) scans correlate with the tumor’s cellularity and proliferative activity (Alexiou et al. 2007). The gold standard to assure diagnosis and accurately identify the respective histological glioma subtype is the operative biopsy with subsequent work-up of the tissue specimens by an experienced neuropathologist.

When planning a therapy, in case of glioblastoma, it is important to know that all therapy strategies are not curative interventions, they are only life-prolonging. Depending on the tumor location and the patient's preoperative Karnofsky score, surgical interventions usually aim at a maximal surgical resection of the tumor without destroying any functional normal tissue. This results in a longer survival and improves the quality of life (Lacroix et al. 2001). Following the operation, the patients receive a combined radio- and chemotherapy. The chemotherapeutic drug of choice is temozolomide. The first published study by Friedman et al. (1998) showed a response rate exceeding 50 % in newly diagnosed glioblastoma patients. Various studies have shown so far that adjuvant application of temozolomide and radiotherapy (Stupp et al. 2005) in combination with a hypermethylated *MGMT* gene promoter (Hegi et al. 2005) is beneficial for a longer survival. New therapeutic strategies involve e.g. angiogenesis inhibitors like bevacizumab (Avastin), but this approach has not yet proven beneficial enough in clinical trials to gain full approval for the treatment of glioblastoma patients within the European Union outside of clinical or experimental trials (Shirai et al. 2011).

1.1.6 Morphology of glioblastomas

1.1.6.1 Macroscopy

Glioblastomas (WHO grade IV) are not clearly circumscribed and present as a mass lesions involving a focal area (mostly unilateral, those in the brainstem can be bilateral). The tumors often occupy much of a lobe or may extend to the corpus callosum or even to the contralateral

hemisphere. The cut surface shows multiforme colours with the tumor mass (greyish), recent and remote haemorrhage (red to brown) and yellowish necrosis. This central necrosis can occupy nearly 90 % of the total neoplasm mass. The majority of glioblastomas are clearly located intraparenchymal with a focus in the white matter, but a contact with the leptomeninges and dura is possible mainly when being located superficially (Cotran et al. 2004).

1.1.6.2 Microscopy

To plan the clinical strategy - choice of therapies, potential adjuvant radiation or chemotherapy - the histological tumor classification, including grading predicting the biological behavior of a neoplasm, is of major importance.

Therefore, the World Health Organization (WHO) published a histological classification system of tumors of the central nervous system (latest edition 2007) that is nowadays used worldwide. Central nervous system tumors are divided in 4 WHO grades (Louis et al. 2007, see Table 1): WHO grade I, e.g. the pilocytic astrocytoma being the most common glioma in early childhood, denotes tumors that only show a low proliferative rate and the feasibility of being cured only by radical and maximal surgical resection, as they grow circumscribed.

WHO grade II tumors are characterized by low proliferative activity but infiltrate healthy surrounding brain parenchyma. Some of these tumors transform to higher grade tumors, e.g. anaplastic astrocytomas or glioblastoma.

WHO grade III neoplasms are characterized by microscopic features of malignancy, e.g. nuclear and cellular atypia (chromatin-rich, polymorphic, disproportion of nuclear-cytoplasm ratio) and an increased mitotic activity, the latter also being indicated by an elevated immunohistochemical proliferation index determined with the proliferation marker *'Ki-67'* (clone Mib1).

Glioblastomas belong to the group of WHO grade IV tumors with high mitotic and proliferative activity. These tumors show a high cellularity as well as often marked cellular and nuclear pleomorphism. In addition, tumor necroses and pathologic blood vessels are located within the tumor mass. Glioblastomas diffusely infiltrate the surrounding ('healthy') brain tissue.

Table 1: WHO classification of tumors of the central nervous system. Classification and grading of the main glioma entities and subtypes (with modifications according to Riemenschneider et al. 2009 and Louis et al. 2007). It should be noted that some less common entities are included in the WHO classification (e.g. pilomyxoid astrocytoma, chordoid glioma, astroblastoma), but these rare generally entities and variants are not part of this dissertation and are therefore not mentioned here.

Tumor type	**WHO grade**
Diffusely infiltrating astrocytic gliomas	
Diffuse astrocytoma	II
Anaplastic astrocytoma	III
Glioblastoma	IV
Astrocytic gliomas with more circumscribed growth	
Pilocytic astrocytoma	I
Pleomorphic xanthoastrocytoma	II
Subendymal giant cellastrocytoma	I
Oligodendrogliomas and mixed gliomas	
Oligodendroglioma	II
Anaplastic oligodendroglioma	III
Oligoastrocytoma	II
Anaplastic oligoastrocytoma	III
Gliomas with ependymal differentiation	
Subependymoma	I
Myxopapillary ependymoma	I
Ependymoma	II
Anaplastic ependymoma	III

1.1.7 Molecular pathology of gliomas

1.1.7.1 Common molecular genetic alterations and cytogenetic changes in different glioma subtypes

Because this dissertation particularly deals with primary and secondary glioblastomas belonging to the diffusely infiltrating astrocytic glioma group (see Table 1), the following paragraphs only discuss molecular genetic alterations and cytogenetic changes that are characterictics for this glioma group.

1.1.7.2 Diffuse astrocytoma (WHO grade II)

Trisomy 7 or a gain of 7q is the most well-known genetic alteration in this glioma subgroup (Nishizaki et al. 1998 and Schröck et al. 1996). Other frequent chromosomal aberrations are mainly losses of 19q (~50 %) and loss of 10p (Reifenberger et al. 2004).

The *TP53* tumor suppressor gene (located on 17q13.1) is mutated in around 60 % of the diffuse astrocytomas. *TP53* mutation is typically associated with a loss of heterozygosity (LOH) on 17q resulting in a complete loss of this tumor suppressor gene. Furthermore about 70 % of diffuse astrocytomas show mutations of codon 132 of the *IDH1 (isocitrate dehydrogenase 1)* gene (Balss et al. 2008) that even appears to be an alteration arising earlier and more common than *TP53* mutations.

Moreover, the $p14^{ARF}$ gene (located on 9p21) is frequently methylated and transcriptionally downregulated in these tumors. Its gene product activates *MDM2 (murine double minute)*-mediated p53 protein degradation (Watanabe et al. 2007). Additional epigenetically silenced genes include the *EMP3 (epithelial membrane protein 3)* gene (located on 19q13.3; Kunitz et al. 2007) that is involved in proliferation and cell-cell interactions, the *MGMT (O^6-methylguanine-DNA methyltransferase)* gene (located on 10q26) that encodes for a DNA repair protein removing alkyl groups from the O^6 position of guanine (Watanabe et al. 2007) and PCDH-gamma-A11 (*protocadherin-gamma subfamily 11*; Waha et al. 2005) located on 5q31. The latter gene encodes a protein normally mediating the synaptic complexness in the developing brain (Noonan et al. 2004). Another frequent alteration is the overexpression of *PDGFRA (platelet-derived growth factor receptor alpha)* (Fleming et al. 1992) encoding for a

cell surface tyrosine kinase receptor for different members of the platelet-derived growth factor family.

1.1.7.3 Anaplastic astrocytoma (WHO grade III)

This glioma subgroup often presents with chromosome 7 gains (Schröck et al. 1996), a loss on chromosome 19q and shows, similar to the group of diffuse astrocytomas, frequent *TP53* and *IDH1* mutations. About 25 % of anaplastic astrocytomas exhibit mutations in the tumor suppressor gene *Rb1 (retinoblastoma 1*; Ichimura et al. 1996). In contrast to glioblastomas, anaplastic astrocytomas do not often show frequent mutations of the *PTEN (phosphatase and tensin homolog)* tumor suppressor gene or allelic losses on 10q. However, alterations of *CDKN2A* and *CDKN2B* tumor suppressor genes, whose gene products (cyclin-dependent kinase inhibitor 2A/B) negatively regulate the cell cycle G1/S-phase transition, are found in a subset of anaplastic astrocytomas (Ichimura et al. 2000).

1.1.7.4 Glioblastoma (WHO grade IV)

Increased insight into the pathogenesis of glioblastomas revealed that within histologically identical glioblastomas two different molecular defined entities exist (Kleihues and Ohgaki et al. 2007). While primary glioblastomas arise *de novo*, secondary glioblastomas develop by progression from a preexisting low-grade diffuse or anaplastic astrocytoma. The latter glioblastomas develop over many months or years and typically affect younger adults (30-45 years). Primary glioblastomas mostly occur in older people (mean, 55 years) and have a shorter clinical history. These tumors do not present with any clinical history of a preexisting precursor lesion. They account for the vast majority of glioblastomas (Kleihues et al. 1999). This differentiation is important, because primary and secondary glioblastomas are distinct in their pattern of molecular genetic changes (see Figure 1).

In general, primary and secondary glioblastomas carry multiple epigenetic aberrations. The main difference between primary and secondary glioblastomas is that more than 65 % of all secondary glioblastomas present mutations within the *TP53* tumor suppressor gene whereas only 30 % of all primary glioblastomas show this genetic alteration (Kleihues et al. 2007; Ichimura et al. 1996).

Primary glioblastomas, however, present with high frequency of *EGFR* amplifications. Nearly 40 % of all patients diagnosed with primary glioblastomas show this amplification. Approximately 50 % of these tumors exhibit receptor-activating mutations in the receptors´ extracellular ligand binding domain resulting in a constitutively activated receptor also in absence of ligand binding (*EGFR* vIII mutant) (Wong et al. 1987, 1992). In addition, primary glioblastomas are characterized by frequent *PTEN* mutations and exhibit *MDM2 or MDM4* amplification. Secondary glioblastomas rarely present these alterations.
In contrast, secondary glioblastoma that develop from lower-grade precursor lesions frequently show *TP53* and *IDH1* mutations (> 66 %; Parsons et al. 2008 and Ohgaki et al. 2007). Furthermore, secondary glioblastomas more commonly exhibit an overexpression of *PDGFRA* and a hypermethylation of *Rb1* than primary glioblastomas do (Ohgaki et al. 2007; Nakamura et al. 2001). *MGMT* and *EMP3* gene silencing has been published as being more frequent in secondary than in primary glioblastomas, whereas the *NDRG2* (*N-myc downstream regulator 2)* gene is more commonly silenced in primary glioblastomas (Ohgaki et al. 2007; Tepel et al. 2008).

In conclusion, primary and secondary glioblastomas represent genetically distinct entities, but share similar histological features and an overall poor prognosis. This may be explainable by the fact that these alterations affect identical signaling pathways, namely the p53, MAPK, PTEN/PI3K/AKT, and Rb1 pathways, and thereby lead to identical functional consequences (Reifenberger et al. 2004; Riemenschneider et al. 2005, 2006).

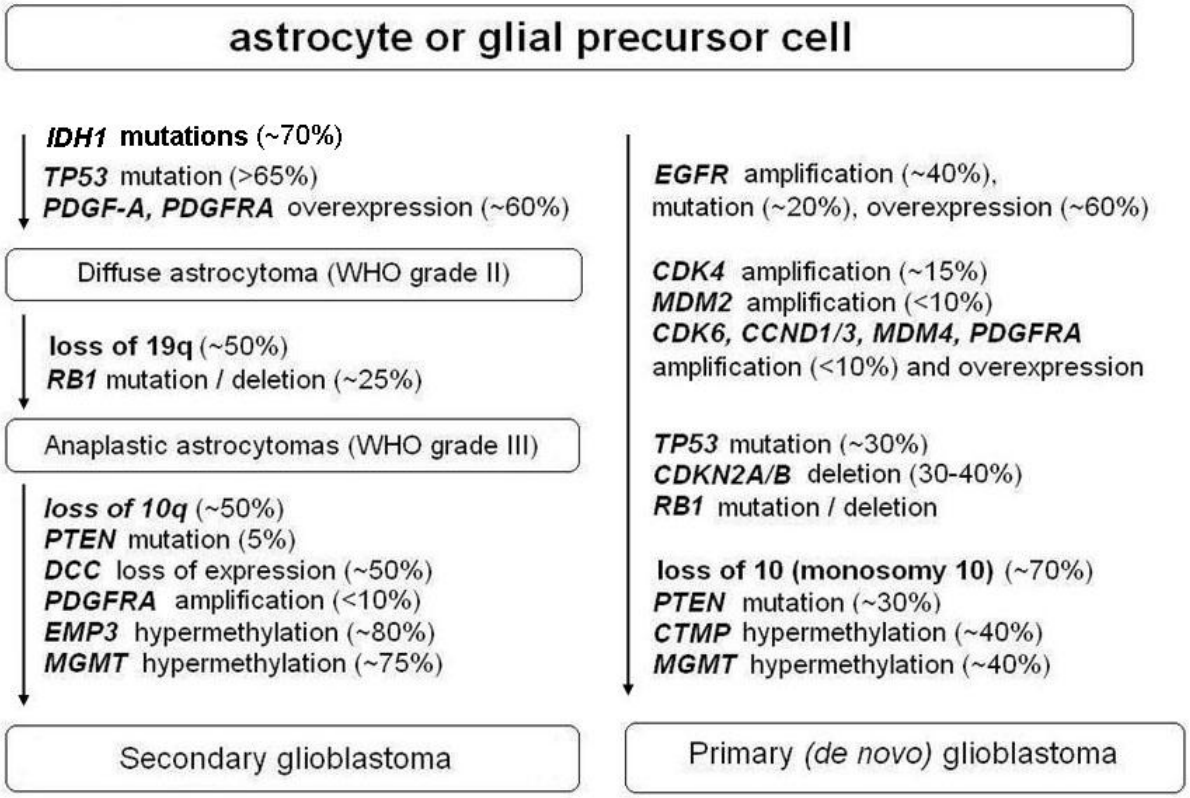

Figure 1: Schematic overview of the molecular changes leading to primary or secondary glioblastomas (adapted from Riemenschneider et al. 2009). Note that genetic alterations are distinct between secondary glioblastoma and primary (*de novo*) glioblastoma (see text for more details).

1.2 *SOCS3* gene and protein

1.2.1 *SOCS3* gene and protein – location and structure

The *SOCS3* (suppressor of cytokine signaling) gene is located on chromosome band 17q25. It consists of 2 exons and 1 intron (Figure 2), which include the entire 3300 basepair coding region. *SOCS3* gene expression is induced by different cytokines (IL6, IL10, IFN-gamma) and acts as a negative regulator of cytokine signalling within the JAK/ STAT pathway.

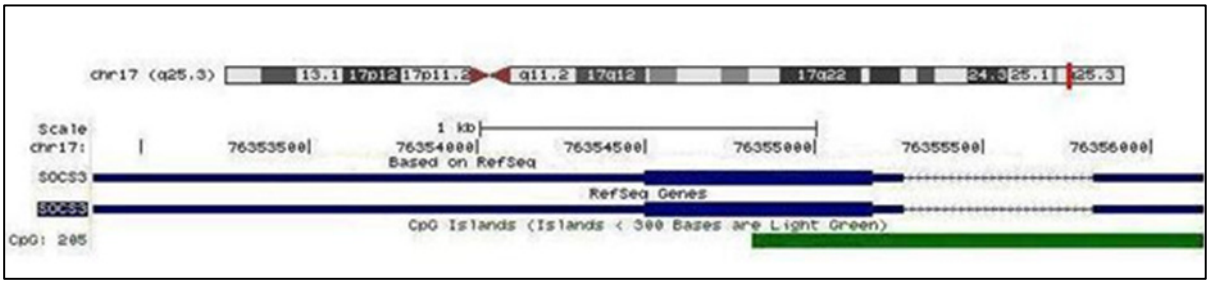

Figure 2: *SOCS3* is located on chromosome band 17q25. *SOCS3* genomic location and the associated CpG island (highlighted green) on chromosome 17q25 (*UCSC Genome Browser, February 2009 Assembly*). *SOCS3* consists of *2* exons and 1 intron and contains a 3300 basepair coding region.

SOCS3 protein belongs to a family of eight structural related proteins: SOCS 1 to 7 and CIS *(Cytokine inducible SH2-containing protein)* (Cooney et al. 2002; Krebs et al. 2000). Each of them contains a central Src-homology (SH2) domain and a specific "SOCS box" at their C-terminal end (Figure 3). The SH2 domain, by which SOCS3 binds to target proteins, functions as a regulatory unit of intracellular signaling pathways by interacting with high affinity to phosphotyrosine-containing target peptides. This affinity is sequence-specific and of an exact phosphorylation-dependent manner. The SOCS box takes part in forming E3 ligase complexes that target proteins for their proteasomal destruction (Piessevaux et al. 2008).

In addition, SOCS 1 and 3 own a “KIR (kinase inhibitor region)” domain at their N-terminal end that acts as a pseudosubstrate of JAK, thus inhibiting kinase activity (Hansen et al. 1999; Nicholson et al. 1999). The SOCS3 protein is located cytoplasmically.

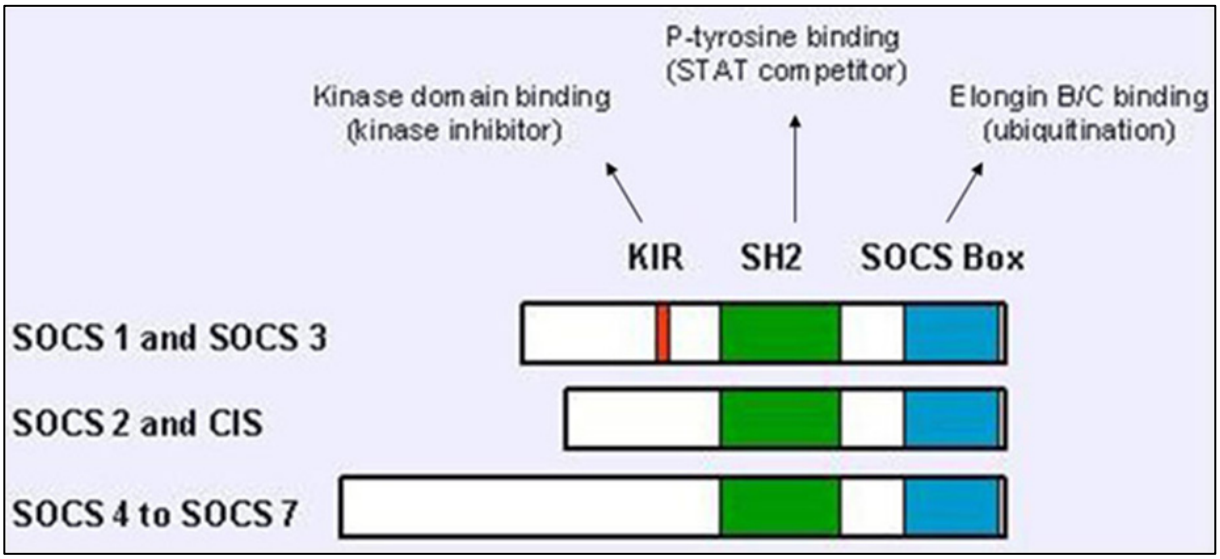

Figure 3: Schematic representation of the structure of SOCS proteins. SOCS3 belongs to a family of eight structural related proteins. These proteins are characterized by the presence of an SH2 central domain and a C-terminal SOCS box. In addition SOCS1 and 3 own a kinase inhibitory region (KIR) at their N-terminal end region. These SOCS proteins interact with phosphotyrosine-phosphorylated proteins by using their central SH2 domain and with E3 ligase complexes/ Elongin BC through the SOCS box (Kamura et al. 1998; with modifications by Elliott et al. 2004).

1.3 JAK/STAT signaling pathway and SOCS3 protein

1.3.1 JAK/STAT signaling pathway

The JAK/STAT signaling pathway conducts information from the extracellular compartment through the cell membrane into the cell nucleus. There, it activates specific target gene promoters on the DNA resulting in DNA transcription. The JAK/STAT pathway system comprises three components: an intramembranous receptor, JAK *(Janus kinase)* and STAT *(Signal transducer and activator of transcription)*. JAK/STAT signaling is induced by a wide variety of cytokines and different growth factors (e.g. EGF protein) leading to diverse cellular functions including growth, cell-proliferation, immunological response and hematopoiesis (Aaronson et al. 2003; O'Shea et al. 2004; Imada 2000; Quesnelle et al. 2007). In various human neoplasms immune derangement and an abnormal constitutive activation of the JAK/STAT pathway has been observed. STAT3, for instance, is permanently activated in several hematologic tumors (Darnell 2005). Inhibitors of JAK-STAT pathways are currently being more and more investigated in the area of oncology and immunology.

1.3.2 SOCS3 protein - function within the JAK/STAT signaling pathway

The *SOCS3* gene product has a lot of different functions, e.g. it is essentially involved in the negative regulation of fetal liver erythropoiesis and hematopoiesis (Marine et al. 1999b) or obesity genesis (Reed et al. 2010). In addition, the SOCS3 protein acts as a regulator controlling for an exorbitant JAK/STAT pathway activation in immunological processes (Figure 4; Cooney et al. 2002) and therefore avoids excessive immunity reaction.

The most interesting function of SOCS3 for physiological processes as well as for tumor development and progression is its influence on the JAK/STAT pathway that is stimulated by a wide variety of cytokines. In general, *SOCS3* mRNA and also SOCS3 protein levels are low in unstimulated cells. After being stimulated by a wide variety of cytokines, *SOCS3* expression is rapidly induced. Cytokine-mediated activation of the JAK/STAT signaling transduction pathway leads to a transcriptional increase of several genes, including SOCS3 that in turn acts as part of a negative feedback loop by inhibiting JAK activity through a mechanism involving receptor association. In detail (see Figure 4): Cytokines bind extracellularly to a receptor complex, which results in an auto-tyrosine phosphorylation of the

intracellularly located receptor-associated Janus kinase (JAK), the cytoplasmic fraction of the cytokine receptor, and STAT. These phosphorylated STATs form an activated dimer and are then translocated to the cell nucleus where they bind to specific DNA sequences and transcription factors to influence target gene transcription. One of these targets is the *SOCS3* gene. The resulting overexpression of SOCS3 protein leads to an inhibition of the JAK/STAT pathway and thereby cytokine signaling. Thus, SOCS3 serves as a crucial regulator controlling for an excessive activation of cytokine-related JAK/STAT signaling (Krebs et al. 2000).

In many human cancers, the JAK/STAT signaling pathway is known to promote oncogenic properties of the cancer cells (Imada et al. 2000; Yu et al. 2009) and SOCS3 - as a negative regulator of this signaling pathway - has been suggested to function as a tumor suppressor (Baltayiannis et al. 2008). As such, inhibition of SOCS3 enhances tumor development, progression or growth in multiple human cancers, including lung and liver carcinomas (Baltayiannis et al. 2008), melanoma (Komyod et al. 2007), breast cancer (Ying et al. 2010; Sasi et al. 2010) and prostate cancer (Puhr et al. 2009), as well as squamous cell carcinoma (Weber et al. 2005). Inactivation of *SOCS3* in cancer cells is commonly caused by promoter hypermethylation (Weber et al. 2005; Fourouclas et al. 2008; He et al. 2003; Sutherland et al. 2004; Tokita et al. 2007). In human glioblastomas, *SOCS3* promoter hypermethylation has been described to correlate with an unfavorable clinical outcome in a series of 46 glioblastoma patients (Martini et al. 2008).

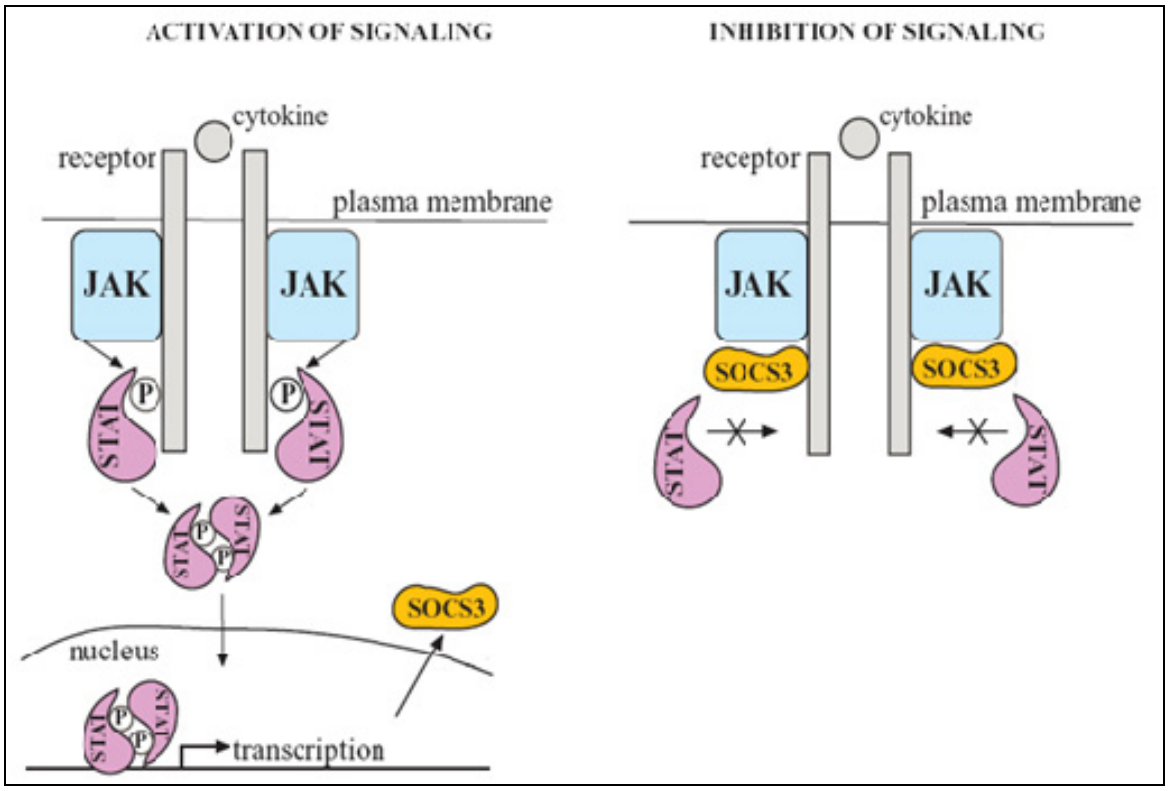

Figure 4: Physiological function of the suppressor of cytokine signaling 3 (SOCS3) protein as an inhibitor of the JAK/STAT pathway. Cytokines bind to the extracellular part of a transmembrane receptor complex, which results in tyrosine phosphorylation of the intracellularly located receptor-associated Janus kinase (JAK), the cytoplasmic fraction of the cytokine receptor and STAT. Phosphorylated STATs form an activated dimer and are then translocated to the cell nucleus where they bind to specific DNA sequences and transcription factors to influence target gene transcription. One of these targets is *SOCS3*. The resulting overexpression of SOCS3 protein leads to an inhibition of the JAK/STAT pathway and cytokine signaling. Thus, SOCS3 is part of a negative feedback loop that prevents excessive JAK/STAT pathway activation (modified from Cooney 2002).

1.4 Research aims of this doctoral thesis

The project was built on the following preliminary results of our research group: In a panel of 30 gliomas comprising 6 glioblastomas and 24 low-grade and anaplastic gliomas (+ 4 non-neoplastic brain tissues used as controls), a virtual absence of *SOCS3* promotor hypermethylation in primary glioblastomas was detected, while *SOCS3* promoter methylation was found in low-grade, anaplastic and secondary glioblastomas. An additional Affymetrix chip-based mRNA expression screen on infiltrating glioma cells showed that *SOCS3* expression was significantly downregulated (Affymetrix sample set 227697_at; fold change = 2.55; *p value* < 0.01) in the invasive glioblastoma cells when compared to the less invasive tumor cells from the solid tumor core. Based on these preliminary findings, two hypotheses were generated and served as a basis for this doctoral thesis (see Figure 5). As primary glioblastomas frequently demonstrate activating *EGFR* aberrations, *SOCS3* methylation might be an alternative mechanism to substitute for the lack of *EGFR* aberrations in low-grade, anaplastic gliomas and secondary glioblastomas. In addition, *SOCS3* inactivation may regulate the invasive phenotype of glioma cells.

In order to follow up on these hypotheses the following experimental steps appeared to be necessary:

1. The tumor panel was extended by an additional set of 16 primary glioblastomas, 8 secondary glioblastomas, and 6 non-neoplastic brain tissues. For these additional samples *SOCS3* promoter methylation analyses were performed using sodium bisulfite sequencing.
2. Single-strand conformation polymorphism (SSCP) analysis was performed to investigate for mutations as another potential inactivation mechanisms of *SOCS3* than promoter hypermethylation.
3. *EGFR* gene copy number and protein expression was assessed by *real-time* (RT) PCR analysis and immunohistochemistry, respectively. These results were correlated to the *SOCS3* promotor methylation status.
4. *SOCS3* function was investigated *in-vitro* after transient transfection (inhibition of *SOCS3* transcription) and later in stable shRNA mediated *SOCS3 knock-down* glioma cell lines.

5. Activation of downstream signaling targets within the EGFR/JAK/STAT pathway was assessed *in-vitro* by means of phosphorylation-specific antibodies in dependence on *SOCS3* inactivation.
6. The functional impact of SOCS3 inactivation on tumor cell invasion, proliferation and apoptosis was investigated by using appropriate cell biological assays *in vitro*.

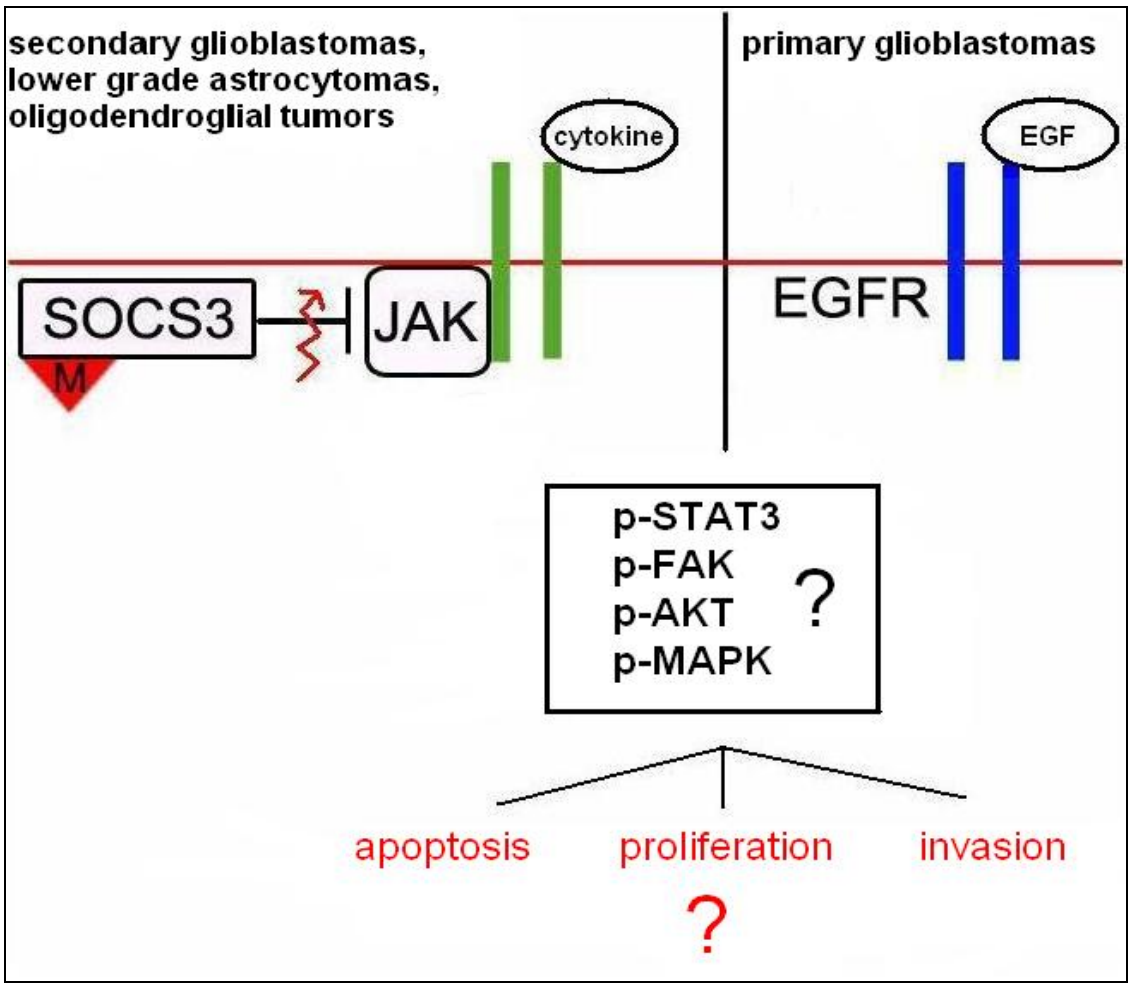

Figure 5: Hypothesis and experimental approach. The major question to be addressed in this work was whether *SOCS3* promotor hypermethylation represents a surrogate mechanism in those glioblastomas that lack aberrantly activated EGF receptor signaling? Does *SOCS3* downregulation lead to the activation of EGFR-related downstream signaling pathway members? To analyze this hypothesis a panel of antibodies against phosphorylation-specific epitope was used and functional cell-based assays were performed.

2 Material

2.1 Tumor samples

Tumors were selected from the tumor tissue collection of the Department of Neuropathology, Heinrich-Heine-University, Düsseldorf, Germany and investigated according to protocols approved by the institutional review board. Tumors were classified according to the criteria of the World Health Organization (WHO) classification of tumors of the central nervous systems (Louis al. 2007). Parts of each tumor were snap-frozen directly after operation and stored at -80 °C. Only tissue samples with a tumor cell content of 80% or more were used for molecular analyses. The tumor series consisted of 60 human gliomas, including 25 primary glioblastomas and 8 secondary glioblastomas, WHO grade IV (*GB*); 4 anaplastic astrocytomas, WHO grade III (*AA*); 3 diffuse astrocytomas, WHO grade II (*A*); 6 anaplastic oligoastrocytomas, WHO grade III (*AOA*); 4 oligoastrocytomas, WHO grade II (*OA*); 7 anaplastic oligodendrogliomas, WHO grade III (*AO*); and 3 oligodendrogliomas, WHO grade II (*O*) (Table 2). Ten non-neoplastic brain samples were taken from different individuals *(NB1-NB10)* and used as reference samples (5 tissue specimens obtained by neurosurgical resection or open biopsy, 2 tissue specimens obtained at autopsy and 3 tissue specimens or nucleic acids obtained from commercial sources; Table 2).

Commercially available hypermethylated DNA (CpG GenomeTM Universal Methylated DNA, Cat.-No. S7821; Millipore, Billerica, MA) was used as a positive control for the methylation studies.

Table 2: Clinical data of the patients included in the study.

Case No.	*SOCS3*	Age	gender	Tissue from*
AOA 18	hypermethylated	33	m	1
OA 6		50	m	1
pGB 115		31	m	1
A 72		44	m	1
AO 34		51	f	1
AOA 15		68	m	1
O 13		61	m	1
OA 1		41	m	1
AOA 10		33	m	1
AO 35		71	m	1
sGB 4		72	m	1
sGB 119		37	m	1
O 18		47	m	1
AA 93		42	f	1
AO 19		47	m	1
OA 2		61	f	1
AO 23		48	m	1
A 78	not hypermethylated	65	m	1
AOA 13		56	m	1
O 14		n.a.	f	1
AO 29		60	f	1
A 8		32	m	1
pGB 130		65	f	1
AA 77		13	m	1
AA 7		n.a.	m	1
pGB 98		54	m	1
OA 9		65	f	1
AO 17		59	m	1
AO 21		61	m	1
AOA 7		50	m	1
AOA 39		69	m	1
AOA 46		37	m	1
pGB 137		57	m	1
pGB 110		69	f	1
pGB 133		52	m	1
pGB 107		74	m	1
pGB 164		49	m	1
pGB 59		71	f	1
pGB 955		69	m	1
pGB 966		67	f	1
pGB 962		43	m	1
pGB1059		54	m	1
pGB 260		53	f	1
pGB 941		43	f	1
pGB 930		52	f	1
pGB 756		57	m	1
pGB 962		43	m	1
pGB 825		76	f	1
pGB 912		78	m	1
pGB 710		74	m	1
pGB 974		54	m	1
pGB 961		72	m	1
pGB 700		73	m	1
pGB 136		63	f	1
sGB 239		50	m	1
sGB 237		39	m	1
sGB 238		29	f	1
sGB 175		62	m	1
sGB 236		59	f	1
sGB 234		45	m	1
HM-DNA	controls	n.a.	m	3
NB1		65	m	1
NB2		72	f	2
NB3		24	m	3
NB4		<1	f	3
NB5		37	m	3
NB6		76	m	2
NB7		n.a.	n.a.	1
NB8		n.a.	n.a.	1
NB9		n.a.	n.a.	1
NB10		n.a.	n.a.	1

*
1, tissue specimens *(tp)* obtained by neurosurgical resection or open biopsy;
2, tissue specimen obtained at autopsy;
3, *tissue specimen* or nucleic acids obtained from commercial sources;
n.a. data not avaliable

2.2 Human glioblastoma cell lines

The following glioblastoma cell lines were used in this study:

Table 3: The TP365MG cell line was provided by professor V.P. Collins, Cambridge, UK and the others were obtained from the American Type Culture Collection, Manassas, VA.

Cell line	Cell type
A172	human glioblastoma cell line
U251MG	human glioblastoma cell line
TP365MG	human glioblastoma cell line
U118MG	human glioblastoma cell line
T98G	human glioblastoma cell line
U87MG	human glioblastoma cell line

2.3 Oligonucleotides

2.3.1 Primers

All primer sequences used in the own experiments are listed in the respective chapters and were obtained from Eurofins MWG, Ebersberg, Germany.

2.3.2 siRNAs and shRNAs

The sequences of the siRNAs (Qiagen, Hilden, Germany) and shRNAs Eurofins MWG, Ebersberg, Germany) used for the transient or stable transfection of cultured glioblastoma cell lines are provided in **Table 4** below.

siRNA (50nM)	sequence (sense strand)
Hs_*SOCS3*_6	5'-cgcucagcgucaagacccatt-3'
Custom siRNA_*SOCS3*	5'-ccaagaaccugcgcauccatt-3'
AllStars Negative Control siRNA	not available
ShRNA	**sequence (sense strand)**
sh1_*SOCS3*	5'-tgacggtcttccgacagagat-3'
sh2_*SOCS3*	5'-tttctcataggagtccaggtg-3'

2.4 Transfection plasmid

ShRNAs were cloned into the pcDNA^{TM} 6.2-GW/EmGFP-miR vector (Invitrogen, Carlsbad, CA; see Figure 6) containing the human cytomegalovirus (CMV) promoter, EmGFP (green fluorescent protein, 26.9 kDa) for fluorescent detection as well as a blasticidin resistance gene for selection of the stably transfected glioblastoma cells.

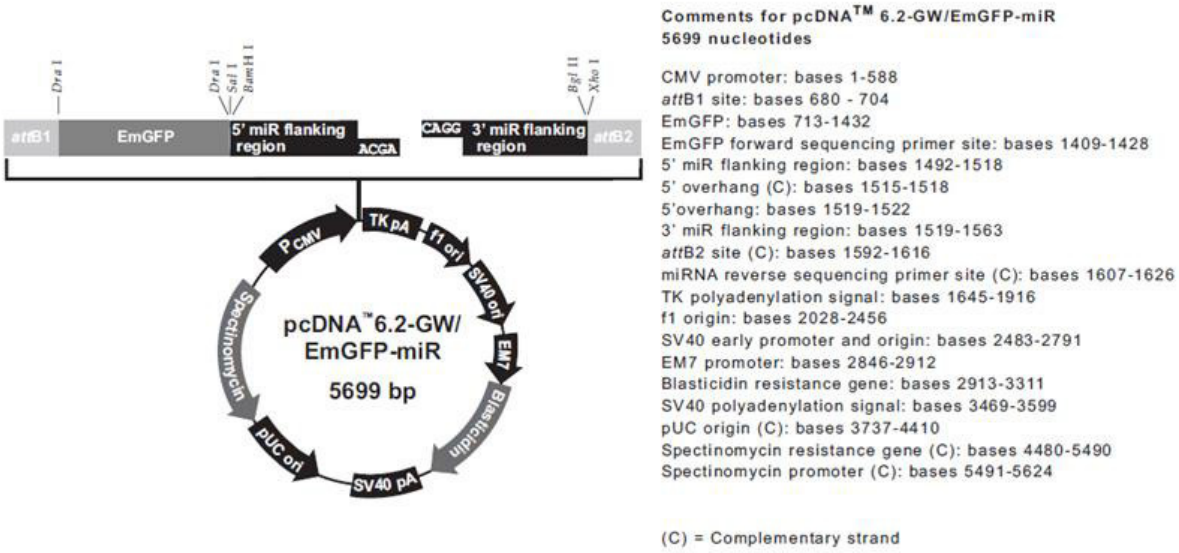

Figure 6: The pcDNA^{TM} 6.2-GW/EmGFP-miR vector (Invitrogen, Carlsbad, CA) used for stable transfection of glioblastoma cell lines. This vector contains the green fluorescence protein (GFP) gene, a blasticidin and spectinomycin resistant gene.

2.5 Antibodies

2.5.1 Primary antibodies

Table 5a lists the different commercially available primary antibodies used in the own experiments and their respective sources.

Table 5a: Primary antibodies and dilutions.

Antibody	Raised in	Dilution	Manufacturer	Catalog No.
p-STAT3 (Tyr705)	Mouse	1:500 in 5 % milk	Cell Signaling	#9138
p-MAPK (Thr202/Tyr204)	Rabbit	1:500 in 5 % BSA	Cell Signaling	#9101
p-Akt (Ser473)	Rabbit	1:1000 in 5 % BSA	Cell Signaling	#4060
p-FAK (Tyr397)	Rabbit	1:500 in 5 % BSA	Cell Signaling	#3283
α-Tubulin	Mouse	1:3000	Sigma-Aldrich	# T5168
SOCS3	Rabbit	1:100	Abcam	#160030

2.5.2 Secondary antibodies

The following secondary antibodies were used for detection of primary antibody binding (Table 5b).

Table 5b: Secondary antibodies and dilutions.

Antibody	conjugat	Dilution	Manufacturer	Catalog No.
Anti-mouse-IgG	HRP	1:10000 in 5 % milk	Jackson Lab	115035174
Anti-rabbit-IgG	HRP	1:10000 in 5 % BSA	Jackson Lab	211032171

2.6 Solutions, buffers and media

The following solutions, buffers and media were used **(Table 6)**:

Solutions, buffers, media	Composition
1 x TE-buffer:	10 mM Tris HCL 1 mM EDTA, pH 8.0
10 x TAE-buffer	400 mM Tris-Base 200 mM NaOAc 10 mM EDTA, pH 8.0
10 x TBE-buffer:	900 mM Tris Base 900 mM Borsäure 20 mM EDTA, pH 8.0
1 x TBST-buffer	18 g NaCl 200 ml Tris-Puffer *Aqua dest.* ad 2000 ml 2 ml Tween
Sequencing-buffer	4 ml not-ionised Formamid (80 % v/v) 1 ml EDTA (25 mM, 20 % v/v, pH 8.0) 250 mg Blue Dextran (50 mg/ml)
6 x Sample loading-buffer (for agarose gels)	30 % Glycerol (in 1 x TE-buffer) 0.025 % Bromophenolblue 0.025 % Xylencyanol
4 x Sample loading-buffer (for SSCP gels)	4 part of formamide 1 part of Bromophenolblue/ Xylencyanol-dilution (Sigma)
Sodium carbonate solution	210 g sodium carbonate 3.5 ml formaldehyde *Aqua dest* ad. 7000 ml
4 x Sample loading-buffer (for SDS page)	100 mM Tris, pH 6.8 6 % SDS 40 % Glycerol, 4 % β-mercaptoethanol 0.025 % Bromphenolblue
Protein-lysis-buffer	50 mM Tris-Cl, pH 8.0 150 mM NaCl 0.5 % TritonX-100 0.5 % Deoxycholate 1 Tablet of protease inhibitor (Roche, Germany) per 10 ml lysis buffer 1 Tablet of phosphatase inhibitor (*PhosStop*, Roche, Germany) per 10 ml lysis buffer
1 x Gel running-buffer	25 mM Tris 250 mM Glycine supplemented with 0.1 % SDS

1 x Transfer-buffer	24 mM Tris 192 mM Glycin 20 % Methanol
PBS-Tween-dilution (containing 0,05 % Tween)	Na_2HPO_4 21.8 g NaH_2PO_4 6.4 g NaCl 180 g *Aqua dest* ad 1000 ml (adjusting pH 7.2) 5 ml Tween 20
4 x SDS buffer	62.5 mM Tris-HCl; pH 6.8 10 % (v/v) Glycerin 2 % (w/v) SDS 0.02 % (w/v) Bromphenolblue
Ponceau S	0.5 % (w/v) in H_2O_{dd} 1% acetic acid
"Stripping" solution for Western blots	2.5 ml 2 M Glycerin 3.2 ml 4 M NaCl 250 µl β-mercaptoethanol 25 µl Tween 20 ad 50 ml Aqua dest.
4 x Stacking gel (pH 6,8)	0.6 M Tris-HCl 0.4 % (w/v) SDS
4 Separating gel (pH 8,8)	25 mM Tris base 0.4 % (w/v) SDS
Freezing-medium for cell culture	10 % (v/v) DMSO 90 % activated fetal calf serum
Complete DMEM (Dulbecco's Modified Eagle's Medium)	DMEM including phenol red 10 % activated fetal calf serum 1 mM sodium pyruvate 100 U/ml Penicillin 100 µg/ml Streptomycin (Cambrex, Belgium) (100µg/ml Blasticidin)
PBS (pH 7,4)	137 mM NaCl 2.7 mM KCl 10 mM Na_2HPO_4 anhydrate 1.8 mM KH_2PO_4

3 Methods

3.1 Molecular biological methods

3.1.1 DNA and RNA isolation

DNA and RNA from frozen tissue specimens (tumor or non neoplastic brain tissue) had been previously extracted by ultracentrifugation as described elsewhere (van den Boom et al. 2003). Total RNA from cultured cells was isolated using the RNeasy mini kit (Qiagen, Hilden, Germany) according to the manufacturer´s protocol.

3.1.2 DNA amplification

DNA amplification was performed by using the polymerase chain reaction (PCR). PCR is one of the easiest and most commonly used biomolecular techniques for the amplification of specific nucleic acid fragments. The reaction mixture contains the double–stranded DNA that shall be replicated, two specific primers (oligonucleotides) with complementary sequences matching to the DNA sequence of interest, reaction buffer and the thermally stable Taq polymerase. Addition and concentration of additives such as $MgCl_2$ (magnesium chloride) and PCR enhancers [Q-Solution or dimethyl sulfoxide (DMSO)] were individually optimized for each primer pair. In addition, annealing temperature and cycle numbers were optimized to aquire the best possible amounts of specific PCR products. A representative example for the master mix of a PCR reaction is listed below (Table 7).

The PCR procedure consists of 3 different steps that are repeated several times: For separating the double-stranded DNA into two single strands *(denaturation)*, the double-stranded DNA is heated to 95 °C. The two single strands are complementary to each other. The next step is called *primer annealing*. Here, it is important to keep a specific temperature (56 °C - 60 °C) permitting the annealing of the primer from the 5' to the 3' end of the DNA. Afterwards, the thermally stable Taq polymerase begins attaching free nucleotides to the 3’ end of the DNA (at 72 °C) and synthesizes the missing complementary DNA strand. So, "new" double

stranded DNA is generated *(extension)*. By the repetition of *denaturation*, *annealing* and *extension* the designated DNA-segment is exponentially amplified.

Table 7: Example for the master mix of a PCR reaction.

	volume (24 µl-Mix)	
Aqua dest	ad 24	µl
10x PCR-buffer	2,5	µl
dNTPs (2mM)	2,5	µl
Primer *forward* (10 pmol)	1,5	µl
Primer *reverse* (10 pmol)	1,5	µl
$MgCl_2$ (Invitrogen)	0,75	µl
Taq-DNA polymerase (Invitrogen, 5 u/µl)	0,1	µl
HotStarTaq DNA Polymerase (Qiagen)	0,15	µl
optionally: DMSO (100 %)	2,5	µl
or Q-Solution (20 %)	5	µl
+ genomic DNA (20ng/µl)	1	µl
Total volume	**25**	**µl**

The whole PCR procedure was performed in a thermocycler (Biometra) using the following program **(Table 8)**:

Step	**temperature**	**duration**	**cycle number**
1. Initial denaturation	95°C	5 min.	
2. Denaturation	95°C	20 sec	x 34
3. Annealing	58°C	20 sec	
4. Extension	72°C	20 sec	
5. Final extension	72°C	10 min.	
6. Hold	4°C	hold	

3.1.2.1 Electrophoretic DNA separation using agarose gels

Using gel electrophoresis, DNA molecules can be separated due to their size. So it is possible to control or analyze the specificity of the amplified DNA. The velocity of migration through the gel depends on size of the DNA fragment and the applied voltage. For agarose gels (2 %) 2 g of agarose powder and 100 ml of 1x TAE buffer were boiled until the resulting solution became clear. Subsequently, ethidium bromide (EtBr; final concentration of 1.0 µg/ml) was added to the solution. EtBr intercalates with DNA and makes it visible in ultraviolet light.

The gel solution was poured into a gel chamber (containing a gel-comb) for polymerisation after cooling to RT for approximately 15 min. DNA samples were supplemented with 6x DNA agarose gel loading buffer and stored up to their application at 4 °C. As soon as the gel was polymerized, it was placed into a gel running-chamber containing 1x TAE buffer, followed by applying the samples into the provided gel pockets. To identify and distinguish all different DNA fragments from each other, 4 µl of a 100 bp (base pair) DNA marker was added to the gel. Electrophoresis was performed at a constant current of 180 mA for 20 min. By using an UV transilluminator all DNA-bands became visible and were photographically documented.

3.1.3 Mutational analysis

Single strand conformation polymorphism (SSCP; Maxam et al. 1980, Orita et al. 1989)/ heteroduplex analysis was performed to detect mutations within the entire coding sequence of *SOCS3* in all 60 tumors. This method is based on detecting differences within the DNA secondary structure. After denaturation, the resulting single strands present modified base pairings depending on their sequence, which results in a specific conformation. These differences are causing different running performances in polyacrylamide gels. At least two different electrophoresis conditions (temperature, cross-linkage of polyacrylamide) were used for each PCR product to increase the likelihood for detection of mutations. Before starting mutation detection for *SOCS3* gene, the parameters were optimized for each PCR product.

For reliably detecting mutations it is absolutely necessary to gain a clear pattern of bands without background. A single mutation within one base leads to a conformational aberration of the single strand resulting in another running performance of the PCR fragment in non-denaturing PAA gels (for mixture of the PAA gel see Table 10; gel stock solution: Acrylamide (AA; 40 %); Bisacrylamide (BAA; 2 %); 10x TBE).

First, *SOCS3* was amplified in 5 fragments from genomic DNA by using PCR (for detailed information concerning PCR conditions see Table 11). This was performed by utilizing 5 different primer pairs that covered the entire coding gene sequence of *SOCS3* (primer sequences are listed in Table 9).

Table 9: Primer sequences used for mutational analysis.

Gene	Application	Annotation	Primer Sequence	Fragment size (bp)
SOCS 3	SSCP analysis	Fragment 1	5'-CTTGTGCTTGTGCCATGTG-3'	200
			5'-GCCACTCTTCAGCATCTCTG-3'	
		Fragment 2	5'-CAGCTGGGTGACTTTCTCAT-3'	216
			5'-CCACCTACTGAACCCTCCTC-3'	
		Fragment 3	5'-CCCGGAGTAGATGTAATAGGC-3'	281
			5'-CGCCACTTCTTCACGCTCA-3'	
		Fragment 4	5'-CAGGTTCTTGGTCCCAGACT-3'	214
			5'-CAAGACCTTCAGCTCCAAGA-3'	
		Fragment 5	5'-GGTCACTGCGCTCCAGTAGAA-3'	264
			5'-CTCGCGCCTTCCTCTC-3'	

All amplified fragments were supplemented with PAA sample loading-buffer (5µl of 6x sample loading-buffer + 5µl DNA-sample). Before applying this mixture to the gel lanes it was heated up to 95 °C (5 min) for denaturation. PCR products were separated by electrophoresis on 10-12 % polyacrylamide gels at RT and at 4 °C overnight. Gels were then silver stained (see Figure 16,) according to the protocol in Table 12 to visualize band patterns. PCR products were sequenced in case of aberrant band patterns.

Table 10: Mixture of PAA-gel, cross-linkage 1(AA):29(BAA), additionally added: 350 µl ammonium persulphate (APS) and 70 µl TEMED to start gel-polymerization.

concentration [%]	**8**	**10**	**12**
volume [ml]:			
AA	38,66	48,34	58
BAA	26,66	33,34	40
TBE (1x)	20	20	20
Aqua dest	114,68	98,32	82

Table 11: PCR-parameters and conditions of gel electrophoresis.

Amplicon	**Primer**	**DNA-fragment (bp)**	**PCR parameters (Temp, cycle number, additives)**	**Gel-parameters (concentration, Temp, Cross-linkage)**
SOCS3 -1	*SOCS3*-SSCP-F1/R1	200	58°C, 35 cycles, Q-Solution	1. 8 %, 4°C, 1:29 2. 10 %, RT, 1:29
SOCS3 -2	*SOCS3*-SSCP-F2/R2	216	58°C, 35 cycles, DMSO	1. 8 %, 4°C, 1:29 2. 10 %, 4°C, 1:29
SOCS3 -3	*SOCS3*-SSCP-F3/R3	281	58°C, 35 cycles, DMSO	1. 8 %, 4°C, 1:29 2. 10 %, 4°C, 1:29
SOCS3 -4	*SOCS3*-SSCP-F4/R4	214	58°C, 35 cycles, Q-Solution	1. 12 %, 4°C, 1:29 2. 10 %, RT , 1:29
SOCS3 -5	*SOCS3*-SSCP-F5/R5	264	58°C, 35 cycles, DMSO	1. 12 %, RT , 1:29 2. 10 %, RT , 1:29

Table 12: Silver staining protocol for SSCP-gels.

Step	Program
1	10 % EtOH for 10 min ***(fixing)***
2	1 % HNO_3 for 2 min
3	Washing with *Aqua dest*
4	***Silver staining*** with 0.2 % $AgNO_3$ for 30 min
5	Washing with *Aqua dest* (two times)
6	Several washing steps with *Aqua dest*
7	$Na_2 CO_3$ (solution for development) washing until band pattern is visualized, (pH-change => **complexed silver ions are reducted to silver**)
8	10 % acetic acid ***(stopping the reaction***) for 10 min
9	Gel is drawn to filter paper, drying in vacuum gel dryer for 2 hours (Biorad)

3.1.4 mRNA expression analysis

3.1.4.1 cDNA synthesis

To perform expression analysis, mRNA was transcribed into cDNA (copy DNA) by using a RNA-dependent DNA polymerase (isolated from retroviral reverse transcriptase). 3 µg of total RNA extracted from tumor tissue or cell lines were added to 29.4 µl RNase-free water and were then denatured at 70 °C in a thermocycler (Biorad) for 5 min followed by a brief ice-quenching.

In the meantime, the RNA-MasterMix was prepared according to the following protocol (**Table 13**):

RNA-MasterMix	1x [µl]	10x [µl]
DTT (dithiothreitol, Invitrogen)	0,4	4
RNasin (40 000 U/l, Promega)	1	10
BSA (bovine serum albumin; 2,9mg/ml)	1,7	17
dNTP-mix (25µM per each dNTP)	2,5	25
pd(N) 6 (1,5µg/µl; Pharmacia)	3	30
5x H-RT-buffer (Invitrogen)	10	100
Total volume	**18,6**	**186**

18.6 µl of prepared RNA-MasterMix were added to the RNA-Mix which was then heated up to 42 °C for 3 min followed by spiking with 1 µl random hexanucleotide primers and SuperScript® Reverse Transcriptase (Invitrogen, Carlsbad, CA). The whole mixture was then incubated using the following program for 60 min (Table 14):

Table 14: Program for cDNA-synthesis.

sequence	time [min.]	temperature [°C]
1.	50	42
2.	10	80
3.	Pause	4

The synthesized cDNA was stored up to use at -20 °C.
Before usage, the cDNA quality was controlled by PCR (PCR conditions are listed in Table 16) with two different ß2-microglobulin primer pairs (for primer sequence see Table 15) that cover an amplicon in the 5' and 3' area of this gene, respectively.

Table 15: Primers used for $ß_2$-microglobulin-PCR.

Gene	Application	Annotation	Primer Sequence	Fragment size (bp)
SOCS 3	*Real-time* (RT) PCR	$ß_2$MG-3-for $ß_2$MG-3-rev	5'-GTTGCTCCACAGGTAGCTCTAG-3'	110
			5'-ACAAGCTTTGAGTGCAAGAGATTG-3'	
		$ß_2$MG-5-for $ß_2$MG-5-rev	5'-GTCTCGCTCCGTGGCCTTAG-3'	123
			5'-CATTCTCTGCTGGATGACGTGAG-3'	

All cDNAs were diluted with *Aqua dest.* (1:25) to perform quantitative mRNA expression analysis by *real-time* RT-PCR.

Table 16a and 16b: PCR-reaction and program for cDNA quality control.

	1x [µl]
Aqua dest.	11.15
5x PCR-buffer	2.5
dNTPs (10 mM)	2.5
Primer *forward* (10 pmol)	1.5
Primer *reverse* (10 pmol)	1.5
$MgCl_2$	0.75
Taq-DNA-polymerase	0.1
Total volume	20

Step	**Temperature [°C]**	**Time [sec]**
1. Initial denaturation	95	300
2. Denaturation*	95	20
3. Annealing*	58	20
4. Extension*	72	20
5. Hold	4	hold

* cycle number: x 30

3.1.4.2 *Real-time* reverse transcription (RT)-PCR analysis

Real-time (RT)-PCR is a quantitative expression analysis that is based on the polymerase chain reaction. In contrast to conventional PCR, the *real-time* (RT)-PCR measures the increase of the PCR product with cycle number and thereby avoids misinterpretation of results caused by saturation.

The double-stranded DNA concentration in this study was measured by incorporation of fluorescent dye *SYBR Green I* intercalating with dsDNA. *SYBR Green I* only shows fluorescence in the presence of dsDNA (double-stranded) and after being specifically stimulated by a halogen lamp (wavelength: 470 nm). *SYBR Green I* absorbs blue light (wavelength: 498 nm) and emits green light (wavelength: 522 nm), which is measured by using a photodiode (Figure 7).

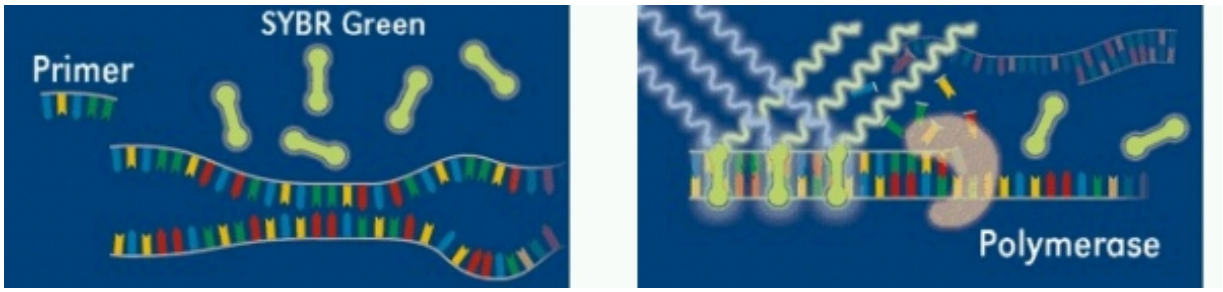

Figure 7: Principle of the *real time* (RT)-PCR method. *SYBR Green I* only binds to dsDNA. The resulting amount of fluorescence is proportional to the (log) amount of the produced dsDNA concentration. (http://homepages.strath.ac.uk/~dfs97113/BB310/lect403.html)

Increases in fluorescence are measured and shown on a monitor after each single PCR cycle. All expression analyses were performed in three technical replicates. Expression of the target gene *SOCS3* was measured against the expression of the house-keeping gene *ARF1* (ADP-ribosylation factor-1; NCBI GenBank no. M36340) using the $\Delta\Delta C_t$ method (Livak et al. 2001). The amount of cDNA utilized for the *real-time* (RT) PCR may slightly vary, i.e. due to an inaccurate quantification of RNA or variable cDNA synthesis efficiency. To correct for these methodical inconsistencies it is necessary to relate all results to a control gene ("housekeeping-gene") which is not regulated in the tumor samples and the expression level of which only depends on the amount of RNA used in the cDNA synthesis reaction. For assessment of *EGFR* gene copy number gains, the amplification level of each gene was normalized to the gene dosage of the genomic marker *D2S1743* (WI3306**.**1) at chromosomal band 2q21.2. Non-neoplastic brain tissue was used as reference for normal tissue (human normal brain). Universal Human Reference RNA (Stratagene) was used on every 96-"well plate" as a calibrator to compare results between individual plates and runs.

To find out the optimal concentration ratio for forward and reverse primer (for used primer sequences see Table 17), it was required to create a "primer matrix".

Table 17: Primer sequences used for *real-time* (RT) PCR.

Gene	Application	Primer Sequence	Fragment size (bp)
SOCS3	*Real-time* (RT)PCR	5'-CAAGGACGGAGACTTCGATT-3'	137
		5'-AACTTGCTGTGGGTGACCAT-3'	
EGFR	*Real-time* (RT) PCR	5'-CACTGCCTCATCTCTCACCATC-3'	109
		5'-GACTCACCGTAGCTCCAGAC-3'	
EGFR genom.	*Real-time* PCR	5'-CACTGCCTCATCTCTCACC-3' 5'-GACTCACCGTAGCTCCAGA-3'	110
ARF	*Real-time* (RT) PCR control	5'-GACCACGATCCTCTACAAGC-3'	111
		5'-TCCCACACAGTGAAGCTGATG-3'	
WI3306.1	*Real-time* (RT) PCR control	5'-CATGACTGCGAGCCCAAGATG-3'	130
		5'-CAGGTGGTGTCATCAGAATCAG-3'	

Table 18: Master Mix for each *real-time* (RT) PCR reaction; ***genom***: genomic.

Reagent/ target gene	***SOCS3*** *(900mM/300mM)*	***ARF1*** *(300mM/300mM)*	***EGFR*** *(300mM/300mM)*	***WI 3306.1*** *(300mM/300mM)*	***EGFR genom*** *(300mM/300mM)*
SYBR Green I dye	12.5 µl	12.5 µl	12.5 µl	12.5 µl	12.5 µl
Primer *rev* (10pmol/µl)	0.75 µl	0.75 µl	0.75 µl	0.75 µl	0.75 µl
Primer *for* (10pmol/µl)	2.25 µl	0.75 µl	0.75 µl	0.75 µl	0.75 µl
Aqua dest	ad 20 µl	ad 20 µl	ad 20 µl	ad 20 µl	ad 20 µl

20 µl of prepared master mix and 5 µl of diluted cDNA solution were pipetted into a 96 – well plate. *Real-time* (RT) PCR was performed by using the StepOnePlus™ sequence detection system (Applied Biosystems, Foster City, CA) with the conditions listed below (step 2&3 were repeated 40 times) in Table 19.

The amount of cDNA exponentially increases during the program. The cycle at which the fluorescence exceeds a detection threshold, the C_t (*threshold* cycle) correlates to the number of target cDNA molecules present in the cDNA added. Correspondingly, the fluorescence of SYBR Green I increases due to the amount of the PCR product and is quantified after each

completed PCR cycle. After finishing the program the relative increase in fluorescence, i.e PCR product is plotted logarithmically against the number of cycles (see Figure 8).

Table 19: *Real-time* (RT) PCR conditions (performed by using StepOnePlusTM sequence detection system).

Step	temperature [°C]	Time
1 Initial denaturation of dsDNA	95	10 min
2 Denaturation	95	15 sec
3 Primer addition, extension and filling up of dsDNA and DNA synthesis	60	1 min

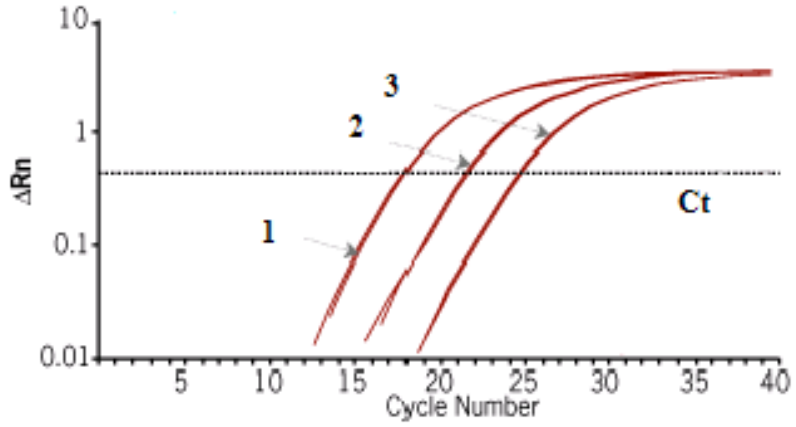

Figure 8: Illustration of product increase (ordinate, ΔRn) versus cycle number (abscissa). This graph shows 3 curves as an example of decreasing fluorescence data from left to right. The more RNA or cDNA the sample contains at the beginning, the smaller is the Ct value. The left curve crosses the threshold (Ct) approximately at the 18th PCR cycle, while the right curve exceeds the threshold at the 25th cycle (Modified from URL: http://www.ambion.com/figs/f01305.gif).

In addition, dissociation and melting temperature curve of the amplicons are considered. Ideally, all samples present a sharp peak at the melting temperature of the revealed amplicon – in contrast in the appropriate blank controls (without template) there should not be any significant fluorescence signals. A fluorescence threshold value ("*threshold cycle*" or C_t

value) is determined for analyzing fluorescence data. The C_t value corresponds to the number of PCR cycles which are necessary to achieve a constantly defined level of fluorescence. By definition, all reaction tubes contain the same amount of synthesized DNA at the point of the C_t value. Calculation of the C_t value - directly deduced from fluorescence raw data or corresponding curves - is used for correcting the background fluorescence. At this detection point of time, the amplification is exponentially. There are no limiting factors (missing oligonucleotids, decreasing enzyme activity or PCR inhibition by accumulation of inhibiting products) during this PCR phase.

For quantification of gene expression, the most commonly used comparative C_t method was applied (Livak et al. 2001). This method involves comparing the C_t values of the samples of interest in case of tumor tissues with a non-neoplastic brain tissue and in case of glioblastoma cell lines with cells transcfected with a scrambled control shRNA, or negative control siRNA. The C_t values of both samples and controls are normalized to the house- keeping gene *ARF1*. Primarily, the relative mRNA expression of the target gene *(SOCS3)* in a sample of interest is quantified to the mRNA expression of the reference gene *(ARF1)*. The software assesses a C_t value (average of three replicates) for each PCR sample followed by determining the difference of the C_t values (average) of target and reference gene (ΔCt). Secondly, the relative expression of the target gene is related to non-neoplastic brain tissue to define $\Delta\Delta C_t$ of the tumor samples as follows: $\Delta\Delta C_t = \Delta C_{t,\ sample} - \Delta C_{t,\ control.}$ So in a logarithmic scale the control values are 0 and all tumor samples are put in relation to the control values. This also allows for comparing measurements between different runs and plates. The relative mRNA expression fold change of *SOCS3* results from reversing the logarithmic values by using the following formula: $2^{-\Delta\Delta Ct}$.

3.1.5 Promotor methylation analysis by using direct bisulfite sequencing

Sequencing of sodium bisulfite modified DNA is often used to analyse the methylation status of CpG sites of interest.

3.1.5.1 Primers and sequenced fragment

The SOCS3 gene is located on the long arm of chromosome 17. Two primers were designed

to span a fragment of the *SOCS3* associated 5'-CpG island located at 17q25.3 between nucleotides 73,867,448 and 73,867,855 (numbering according to the UCSC genome browser, URL: http://www.genome.ucsc.edu). This fragment was PCR-amplified after sodium bisulfite-modification of the DNA using the primers as reported in Table 20.

The amplified fragment covered in total 43 CpG sites, directly spanning the transcription start site of *SOCS3* (see Figure 9). The CpG sites are numbered in relation to the transcription start site starting with positive numbering at the transcription start site in direction to the 3' end and negatively continueing to the 5' end. Thus, the primers are located directly behind the CpG site +27 and -16.

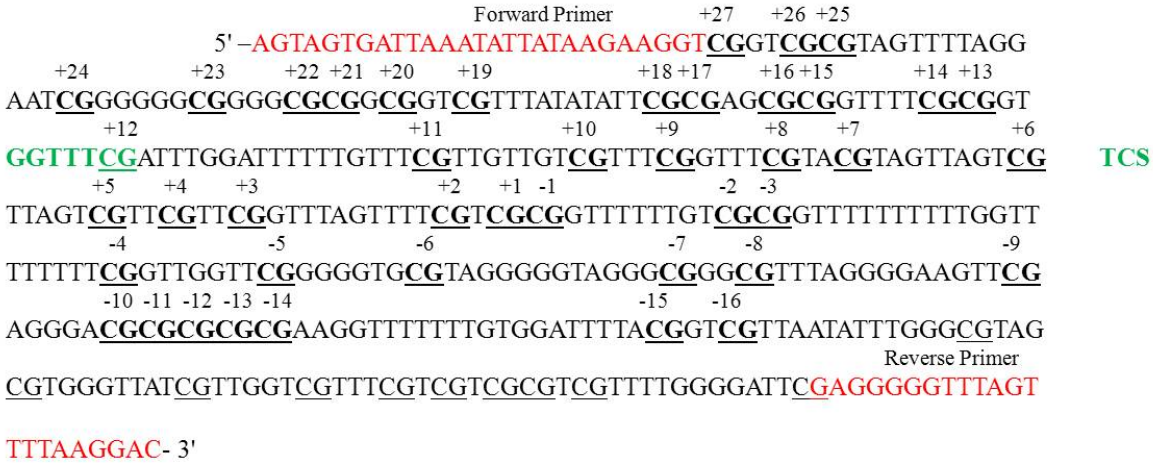

Figure 9: Sequenced fragment of the *SOCS3* 5' gene region and all 43 CpG sites. Transcription start is abbreviated as "TCS" and highlighted green, binding sites for the forward and reverse primer are highlighted in red.

Table 20: Primer sequences used for methylation analysis.

Gene	Application	Primer Sequence	Fragment size (bp)
SOCS 3	Sodium bisulfite sequencing	5'-AGTAGTGATTAAATATTATAAGAAGGT-3'	407
		5'-TCCTTAAAACTAAACCCCCTC -3'	

3.1.5.2 Sodium bisulfite treatment of genomic DNA

Sodium bisulfite preferentially deaminates cytosines (C) into uracils (U), in comparison to a very slow fraction of deamination of 5-methyl-cytosine to thymine (T). Converting genomic DNA by using sodium bisulfite is based upon a method firstly described by Frommer et al. (1992).

The bisulfite reaction results in DNA strands that are no longer complementary to each other. Therefore, it is possible to design specific PCR primers that are only able to bind to one of the bisulfite-treated DNA strands. Specifically designed primers for each single-strand vary in every position where there is a "C" in the original sequence. In case of methylated DNA "C"s that are part of a "CG" dinucleotide remain unchanged and can therefore be detected by sequencing. Bisulfite modification thus serves to transpose an epigenetic difference in a genomic sequence difference that can be readily detected. Unmethylated "Cs" are transferred into "U"s whereas methylated "C"s remained unconverted (see Figure 10a). The next step consists in the PCR amplification of the bisulfite-treated DNA. During this step, uracils are replaced by (see Figure 10b).

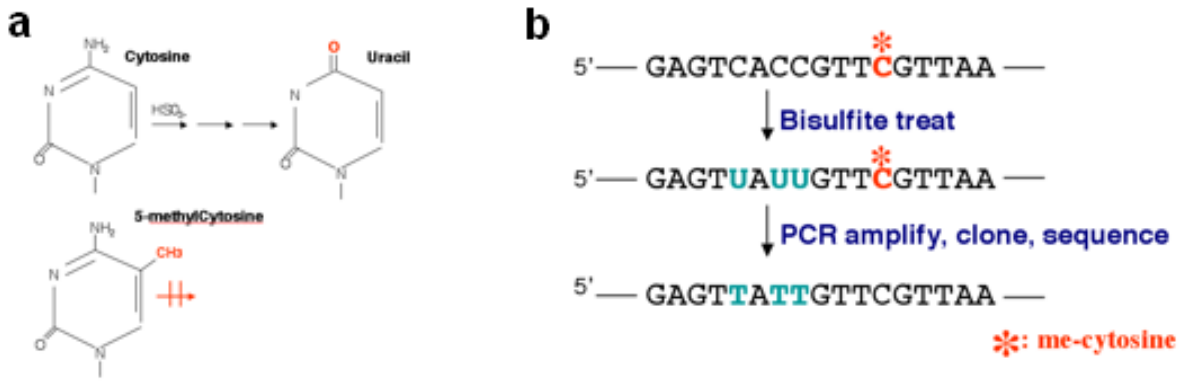

Figure 10: Sodium bisulfite treatment changes unmethylated cytosines into uracils whereas methylated cytosines remain unconverted **(a)**. All bisulfite-converted uracils are replaced by thymines during amplification **(b)**. (URL: http://www.alphabiolab.com/page2/page2.html)

In a direct sequencing method, all obtained trace files of heterogeneously methylated CpG sites show both, cytosine signals for methylated sites and thymine signals for unmethylated

sites. All produced bisulfite-treated DNA is directly used for methylation-specific PCR or stored at –20 °C.

Different solutions were freshly prepared before starting experiments (Table 21). To avoid all feasible sources of contamination special micropipettes were only used for bisulfite sequencing. All solutions were prepared in a separate room under a laminar airflow bench.

Table 21: Solutions used for sodium bisulfite treatment of DNA.

Solution	Ingredients
10 N NaOH	4 g NaOH 10 ml *Aqua dest.*
10 mM hydroquinone	0 11 g hydroquinone 100 ml *Aqua dest.*
3 M sodium bisulfite, pH 5.0	15.6 g 3 M sodium bisulfite (pH 5.0) 50 ml *Aqua dest.*

Sodium bisulfite treatment of 1 µg DNA was performed overnight (16 h) according to the following protocol (Mueller et al. 2007; Table 22):

Table 22: Protocol for bisulfite treatment.

Step	Mixture	Temperature [°C]	Time
1	1 µg DNA + 1.5 µl 10 N NaOH + 38.5 µl *Aqua dest.*	37	15 min
2	15 µl 10mM hydroquinone + 520 µl 3M sodium bisulfite	55	16 h

3.1.5.3 PCR amplification using *SOCS3* primer pairs

Genomic (bisulfite treated) DNA amplification was carried out using the HotStar Taq DNA polymerase kit (Qiagen, Hilden, Germany) with 10 ng of genomic DNA and gene specific primers (see above). The PCR reaction was performed in a standard PCR-Mix and a final volume of 20 µl. PCR products were then used for gel electrophoresis on a 2 % agarose gel and stained with 2 µl EtBr in 1 x TBE buffer. The expected primer specific bands were

identified and eventually cut out from the agarose gel while visualising the PCR products under 313 nm UV light.

3.1.5.4 PCR-purification

PCR products gained from amplification were directly purified after performing gel electrophoresis and cutting-off the bands (180V, 2 %). For this, the following kits were used according to the manufacturer's protocols:

	Manufacturer	**Product**
Gel Extraction Kit	Genomed	Jetquick Gel Extraction Spin Kit
PCR-Purification Kit	Genomed	Jetquick PCR Product Purification Spin Kit

Purified DNA was eluted in 20 µl of sterile *Aqua dest*. (preheated). The purified DNA was stored up to use at -20 °C.

3.1.5.5 Sequencing of DNA fragments

The chain-termination method is also called the Sanger dideoxy-method (*"dd"*-method) developed by Sanger F et al. 1977. This method is an enzymatic synthesis method that uses dideoxynucleotide triphosphate (*ddNTPs*) as DNA chain terminators.
The chain-termination method requires a single-stranded DNA sample, DNA primers, spanning the fragment of interest, a DNA polymerase, fluorescently labelled nucleotides, and specific modified nucleotides that interrupt DNA strand elongation.
Big Dye® solution (Applied Biosystems) is added to each reaction mix that contains all 4 labelled *ddNTPs* (ddATP, ddGTP, ddCTP, or ddTTP). Thus, sequencing is possible in a single reaction. The nucleotides lack the 3'-OH group that is required for forming a phosphodiester bond between two nucleotides. Therefore DNA-strand extension is terminated. All resulting DNA fragments are of varying length. Every single *ddNTP* emits light at different wavelengths. The different fluorescent colors are identified by a detector (ABI-PRISM^{TM}-System). Finally, the base sequence can be read in an electropherogram.

3.1.5.6 Sequencing reaction

5 µl of purified DNA and 5 µl loading buffer were then used for electrophoresis on a 2 % agarose gel and stained with 2 µl EtBr in 1 x TBE buffer to estimate concentration of the PCR-product. 4 to 7.5 µl product were used for the following sequencing reaction (depending on the bands intensity, Table 23):

Table 23: Sequencing Mix.

Purified PCR-product	4-7.5 µl
Reverse Primer (10 pmol/µl)	0.5 µl
Big Dye® Terminator Cycle Sequencing Mix	2.0 µl
Aqua dest.	ad 10 µl

The sequencing reaction was performed using the following program (25 cycles, Table 24):

Table 24: Sequencing reaction performed in a thermocycler (Biometra).

1.	96°C	10 sec
2.	50°C	5sec
3.	60°C	4 min
4.	4°C	Hold

To separate non-inserted fluorescently labelled *ddNTPs*, the sequencing reaction was centrifuged (20 min, 14000 rpm, 4 °C) after addition of 1 µl 3 M of sodium acetate (pH 4.6) and 25 ml 95 % ethanol. The supernatant was removed. The resulting pellet was washed by using 200 µl of 70 % ethanol twice. Subsequently, the DNA pellet was dried and diluted in 4 µl sequencing buffer (for the composition of the sequencing buffer compare Table 6 in 4.6).

3.1.5.7 PAAgel electrophoresis using the DNA sequencer ABI-PRISM™ 377

2 µl of the diluted DNA pellet was applied to a denaturing PAA gel (mixture listed below, Table 25):

Table 25: Composition of the denatured PAA gel.

Urea	21 g
30% acrylamide/bis-acrylamide (29:1)	8.4 ml
10x TBE	6 ml
Aqua dest.	20 ml
10% APS	350 µl
TEMED	15 µl

APS and TEMED were added to the gel mixture shortly before pouring the gel to start polymerization. The glass plates have to be spring-cleaned by utilizing special non-fluorescent cloths with distilled water and isopropanol. This is important, because the sequencer's laser should only recognize the fluorescently labelled nucleotides. After completed gel polymerization the samples were loaded and gel-running was started by utilization of semi-automatic sequence ABI Prism 377 (Applied Biosystems).
The samples' separation was performed at 2500 volts, 48 watts and 51 °C gel temperature for 8 hours. When reaching the region of detecting fluorescence, the laser records fluorescence and generates the electropherogram. While the gel is still running, the sequencing software creates an imaginary gel picture and analyzes this automatically. Finally, all electropherograms were printed and manually analyzed for the presence of methylated CpG dinucleotids.

3.1.5.8 Semiquantitative analysis of methylation

As a result of the inserted DNA mixture even completely methylated tumors might show a weak unmethylated signal after homogenization, resulting from unmethylated intratumoral vessels or contaminating microglial cells. The CpG methylation differences within the single strands are shown as a double peak, consisting of cytosine and thymine, in the electropherogram.
Direct bisulfite sequencing and semiquantitative calculation of a promoter methylation score were carried out as previously established (Tepel et al. 2008). The methylation status at each of the analyzed CpG sites was semi-quantitatively rated (depending on the ratio of cytosine peak to thymine peak height) using the following scale: 0, completely unmethylated; 1, a

weakly methylated signal detectable in the sequence; 2, methylated signal approximately equal to unmethylated signal; 3, methylated signal markedly stronger than unmethylated signal (see example in Figure 11).

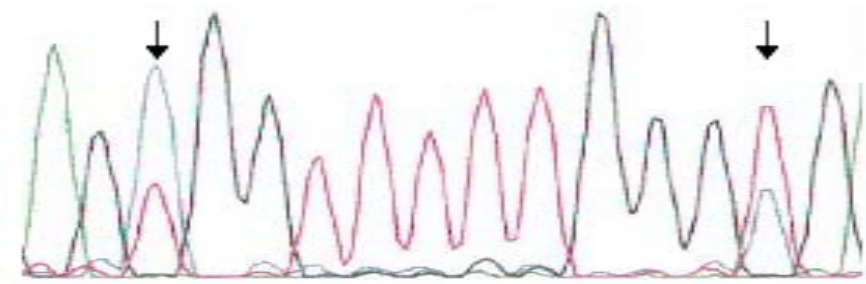

Figure 11: This excerpt shows two "arrow-marked" cytosine-thymine double peaks resulting from sequencing. These are CpG sites, followed by a black guanine. In the first case, blue cytosine outweighs the red thymine (methylation score: 3). In the other double peak the ratio between "C" and "T" is reversed (methylation score: 1).

Based on this rating, a promoter methylation score in per cent was calculated for each tumor as well as for the non-neoplastic brain tissue controls by adding the numbers determined at the individual CpG sites divided by the maximum possible methylation score at all analyzed CpG sites. Tumors with a methylation score exceeding that of non-neoplastic brain tissue were regarded as being hypermethylated (see Figure 13).

False positive results due to incomplete bisulfite conversion were excluded by controlling for the conversion of cytosines entrapped in the respectives sequences that were not part of CG dinucleotides. Only sequences with 100 % conversion rates were used for evaluation.

3.2 Cell biological methods

3.2.1 Cell lines and cell culture conditions

The six glioma cell lines A172, U251MG, TP365MG, U118MG, T98G and U87MG were cultured under standard conditions in Dulbecco´s modified Eagle´s medium (DMEM; Invitrogen, Karlsruhe, Germany) supplemented with 10 % heat-inactivated fetal bovine serum (FCS) and 1 % penicillin/streptomycin (P/S; Invitrogen/GIBCO, Carlsbad, CA) in a 5 % CO_2 containing humidified (95 %) incubator at 37 °C. Cells were passaged under sterile conditions in a laminar airflow bench.

3.2.2 Mycoplasma test

All cell lines were regularly tested for contamination with mycoplasma by nested PCR. Nested PCR is a modified PCR method that - due to the amplification of primer binding sites – is sensitive enough to detect even small amounts of DNA, in this case resulting from contamination with mycoplasma. PCR products were separated using agarose gel electrophoresis (primer sequences are listed in Table 26).

Table 26: Primer sequences used for the mycoplasma contamination test.

Gene	Application	Annotation	Primer Sequence	fragment size (bp)
Mycoplasma	myc-PCR	F1/ R1	5'-ACACCATGGGAGCTGGTAAT-3' 5'-GTTCTTTGAAAACTGAAT-3'	*
Mycoplasma	myc-PCR	F2/ R2	5'-CTTCWTCGACTTYCAGACCCAAGGCAT-3' 5'-GCATCCACCAWAWACTCT-3'	*

*myc-primer are non-specific primer, you can even amplify different strains

3.2.3 Transfection of cultured glioma cell lines

Transfection is the procedure of inserting "external" DNA in a system of choice (here eucaryotic cells) with or without using a vector. Expressing "external" DNA enables to observe the effect / function of this gene on gene expression, transcription, translation and post-translational protein modification. While the transfected DNA is only temporarily expressed in the cells when using a transient transfection method, the so-called "stable"

transfection is characterized by permanently integrating the "external" nucleic acids into the cell´s genome. This results in changed protein expression levels lasting unlimited time.
The transfer of negatively charged DNA through the negatively charged cell lipid membrane is a general problem of transfection. This requires transfection reagents (lipid-based) surrounding the DNA-molecules and so mediating the DNA´s transfer through the cell´s membrane.

3.2.3.1 Transient transfection of glioblastoma cell lines with siRNA

"RNA interference" is a method of "switching-off" genes at the mRNA level. Short double-stranded RNA fragments (siRNAs) are transfected into the cells activating cell endonucleases that specifically cut mRNA complementary to the siRNA. In the own experiments, *SOCS3* was down regulated in A172, U251MG, TP365MG, U118MG, T98G and U87MG glioma cell lines by transient transfection using a 50 nM siRNA (sequence previously published by Puhr et al. 2010) and another commercially presynthesized siRNA (Qiagen, Hilden, Germany) with HiPerFect transfection reagent (Qiagen. Hilden, Germany) (for siRNA sequences see Table 4, 4.2.2 "Material"). Cells were trypsinized and disseminated in a concentration of 3x 10^4 cells/ well on a 24-well plate.
Then 100 µl OptiMEM (serum-free; Invitrogen, Karlsruhe, Germany) and 1.25 µl (50 nM) siRNA (Qiagen, Hilden, Germany) were added and mixed with 3 µl HiPerFect (Qiagen, Hilden, Germany). Followed by an incubation time of 5-10 minutes, the mixture was carefully pipetted onto the cells. After 24 hours the cells medium was changed and after 48 hours cells were harvested and RNA was isolated using the RNeasy mini kit (Qiagen, Hilden, Germany). To normalize for side effects that have not been caused by a specific siRNA-mediated gene knock-down, cells were additionally transfected with commercially available negative control (AllStars Negative Control, Qiagen) used in the same concentration. Results were reproduced in at least two independent experiments.

3.2.3.2 Generation of glioblastoma cell lines with stable *SOCS3 knock-down*

To obtain stably transfected glioblastoma cells, the pcDNA^{TM} 6.2-GW/EmGFP-miR vector (Invitrogen, Carlsbad, CA) was used (for further details see: Figure1, Materials).

Basically, following the protocol of transient transfection, stable transfected cells are exposed to selection pressure by incubation with DMEM containing blasticidin (20 µg/ml) after transfection. Blasticidin interacts by inhibiting peptide bond formation by the ribosome, thereby causing that cells can no longer assemble new proteins through translation. Cells containing the vector are resistant to the blasticidin effect.

Glioblastoma cells with a stable *SOCS3 knock-down* were generated using vector-based shRNA-mediated RNAi. To control for potential off-target effects, two different predesigned shRNA oligonucleotides (Qiagen, Hilden, Germany; sequences listed in Table 2, Materials) were used. Firstly, shRNA oligonucleotides were cloned into the pcDNA^{TM} 6.2-GW/EmGFP-miR vector (Invitrogen, Carlsbad, CA). Then DNA sequencing was performed to confirm the proper orientation of these inserts in the vector and to exclude feasible mutations. Secondly, 320000 cells/ "24-well" of U251MG, U87 and A172 cells were disseminated in DMEM supplemented with 10 % FCS, blasticidin (20 µg/ ml) and without 1 % P/S one day before transfection. The next day, disseminated cells were transfected with the shRNA oligonucleotid-containing pcDNA^{TM} 6.2-GW/EmGFP-miR vectors using GeneJuice transfection reagent (Merck, Darmstadt, Germany) and OptiMEM according to the manufacturer's recommendations. Cells were also transfected with the pcDNA^{TM} 6.2-GW/EmGFP-miR-negative control plasmid containing an insert that can form a hairpin structure that is processed into mature miRNA, but is not predicted to target any known vertebrate gene. The third day, all transfected cells were passaged and seeded in low cell density (10000-50000 cells, depending on the transfection efficiency) in cell culture dishes (10 cm) using DMEM (containing: 10 % FCS, 1 % P/S, blasticidin 20 µg/ ml). The medium was replaced with fresh media every 2-3 days. Only cells that have stably integrated the pcDNA^{TM} 6.2-GW/EmGFP-miR vector survive under these conditions.

Individual clones were then grown from single blasticidin-resistent cell colonies that were isolated by using a pipette. Stable transfectants were further selected by growing under 20 µg/ml blasticidin. Two different subclones of each of the two hairpins were investigated in the *in vitro* experiments to control for insertion-site specific side effects (see Figure 3, Results).

3.2.4 Cell-based functional assays

3.2.4.1 Proliferation assay

To determine the influence of shRNA-mediated *SOCS3* knock-down on cell proliferation, U251MG clones were compared to control-transfected cells using a commercially available BrdU incorporation assay (Roche, Mannheim, Germany). 2000 cells/ 100 µl were seeded on a 96-well plate and incubated with BrdU labeling solution (diluted 1:100 with DMEM) for 24 h at 37 °C. After incubation, cells were fixed according to the manufacturer´s recommendation. Absorption values of the colorimetric reaction were measured on a photometer (370 nm) after incubation with BrdU substrate solution at predefined timepoints (5, 10, 20, 30, 40 min).

3.2.4.2 Apoptosis assay

Apoptotic activity in *SOCS3*-depleted cells and controls was assessed by using a fluorometric caspase-3/7 assay (Promega, Mannheim, Germany) according to the manufacturer´s protocol. 5000 U251MG cells/ 100 µl were seeded to a 96-well plate and incubated at 37 °C for 24 h before performing the caspase-3/7 assay. Fluorimetric measurements (485 nm extinction/530 nm emission; fluorescein-filter) were optimized for the U251MG cell line and performed after 150 minutes of incubation with the caspase substrate at RT.

3.2.4.3 Cell invasion assay

For investigating the impact of *SOCS3* inactivation on the invasive properties of glioblastoma cells, a 24-well modified Boyden chamber assay was used (BD Biosciences, San Jose, CA). The assay is based on a chamber consisting of two medium-filled compartments that are separated by a Matrigel™-coated fluorescence blocking membrane with 8.0 µm pores (Figure 12). After serum-starvation for 24 h cells (500 µl of a 70000 cells/ ml suspension) were seeded into inserts of the upper compartment (containing DMEM, but lacking 10 % FCS). Pores at the insert´s bottom additionally covered with extracellular matrix substances (Matrigel™) allowed the cells to invade into the lower compartment. This compartment contains DMEM supplemented with 10 % FCS a chemoattractant (Figure 12b). After incubation at 37 °C for 24 h, cells that had not invaded were removed and the membrane was

fixed in paraformaldehyde (4 % in PBS) and stained with 4'-6-Diamidino-2-phenylindole (DAPI). Membranes were then sliced out from the inserts and fixed on glass slides. The number of invaded cells was determined by counting the cells on the bottom of the membrane.

Figure 12a and 12b: This figure shows the principle of modified Boyden chamber assay. 24well; BD Biosciences, San Jose, CA. (modified from URL: http://www.bioscience.org/).

All cell-based functional assays (including proliferation, apoptosis and invasion) were performed in at least two completely independent experiments each consisting of at least six replicates (see Figure 20).

3.3 Protein-biochemical methods

3.3.1 Western blot analysis

3.3.1.1 Cell lysis

U251MG cells were harvested, washed with ice-cold 1x TBS twice, and lysed in 500 µl lysis buffer per 10 cm dish (for ingredients see Table 6, "Material"). Special attention was put to the cells` washing with 1x TBS and not with 1x PBS, because phosphorylation status of different proteins should be retained. Phosphate groups of PBS otherwise would have distorted results. *Phospho-STOP* (Roche, Grenzach-Wyhlen, Germany) and a protease inhibitor (Roche, Grenzach-Wyhlen, Germany) were added to the cells to prevent them from dephosphorylation and to inhibit the degradation of proteins.
Cell lysates were shaken on ice for 15 min. Thereafter, the cell lysate was centrifuged at 14000 rounds per minute at 4 °C for 15 min to remove cell debris. The resulting supernatant was subjected to quantification of the total protein concentration using the Bradford method.

3.3.1.2 Protein quantification

The protein concentration of extracted proteins was determined by using the standard Bradford protocol (Bradford MM 1976) and Bradford Protein Assay Reagent® (Bio-Rad, Germany). Bovine serum albumin (BSA, 0-2 mg/ml) was used as protein standard.

3.3.1.3 Sodium Dodecyl Sulfate - Polyacrylamide Gel Electrophoresis (SDS-PAGE)

SDS-PAGE is a method to separate proteins according to their molecular weight and is based on the Laemmli protocol (Laemmli 1970).
Proteins (30 µg) extracted from transfected and control cells were denatured (95 °C, 5 min) and separated by discontinuous SDS-PAGE on 10-12 % acrylamide gels. Samples were diluted in 4× sample loading buffer (see 4.6: Dilutions, buffers, media). As a molecular weight marker, PageRuler™ Prestained Protein Ladder (Fermentas, Germany) was used. Gels were run at 120 V for 90 min.

3.3.1.4 Western blotting

Separated proteins were transferred to nitrocellulose membranes (Burnette 1981, Towbin et al. 1979) (Whatman, Maidstone, UK) using an electrophoretic Trans Blot Cell Blot module (Bio-Rad). After electrophoresis nitrocellulose membranes, blotting pads and filters were wetted in 1x transfer-buffer (for ingredients see Table 6), the components were placed into the Trans Blot module due to the manufacturer's instructions. Transfer was performed at a constant current of 180 mA for 40 min. Transfer was confirmed afterwards by staining the nitrocellulose membranes for 5 min with Ponceau S. The membrane was blocked with 5 % non-fat dry milk or 4 % BSA in TBS-T (for ingredients see Table 6) for 90 min at RT.

After blocking, the membrane was incubated overnight at 4 °C by using the following primary antibodies (all antibodies dilutions are listed in Table 5a/b, "Material"): phospho-STAT3 (phosphorylated on Tyr705), phospho-MAPK (Thr202/Tyr204), phospho-Akt (Ser473), phospho-FAK (Tyr397) and α-Tubulin as a loading control. Primary antibody binding was detected by anti-mouse or anti-rabbit antibodies (for dilution see Table 5b, "Material") linked to horseradish peroxidase for 2 h at RT.

To visualize primary antibody binding by chemiluminescence, the membranes were treated with Immobilon® Western HRP Substrate containing luminol and peroxide solution (Millipore, Billerica, MA) and recorded with the LAS-3000 mini system (Fujifilm Life Science, Stanford, CT). Band intensities were analysed using the ImageJ software comparing protein expression in *SOCS3*-depleted cell lines to control cell lines and using α-tubulin as a loading control. Results were reproduced in at least two independent experiments (see Figure 19). On occasion, incubated nitrocellulose membranes were used again after removal of the bound antibodies ("stripping"). Membranes were incubated in a "stripping" solution (for composition see Table 6) for 30 min at RT. After washing with TBS-T twice, blocking and antibody binding could be reiterated. Results were reproduced in at least two independent experiments (see Figure 19).

3.3.2 Immunohistochemistry

Immunohistochemistry was performed on formalin-fixed paraffin-embedded tissue sections (4 µm; one representative tissue block per patient) of 51 gliomas of different WHO grades.

Paraffin blocks were retrieved from the archive of the Department of Neuropathology, Heinrich-Heine-University, Düsseldorf, Germany.

3.3.2.1 Analysis of EGFR protein expression using immunohistochemistry

After deparaffinization and rehydration (20 min), the tumor tissue sections were pre-treated with Pronase K (Roche, Germany) for 10 minutes and 0.3 % H_2O_2/ PBS (pH 7.4) for 10 minutes to quench endogenous peroxidase activity. After washing the slides in PBS, the primary antibody against EGFR (epidermal growth factor receptor; mouse monoclonal antibody clone E30; Dako, Hamburg, Germany; 1:25 dilution) was applied on the slides and incubated for 30 minutes at RT. After secondary antibody binding immunoreactivity was detected with the EnVision™ Detection System (Dako) using 3,3′-diaminobenzidine tetrahydrochloride (DAB) as a chromogen due to the manufacturer's instructions. Finally, the slides were counterstained in hematoxylin, cleared and coverslipped. Immunoreactivity was quantified as described in 5.3.2.3.
Negative controls without primary antibodies were performed for all reactions. All reagent conditions, temperatures, incubation times and antigen retrieval were identical for each tumor to reach comparable results.

3.3.2.2 SOCS3 protein expression using immunohistochemistry

The tumor slides were pre-treated with 0.3 % H_2O_2/ PBS (pH 7.4) for 10 minutes and washed in PBS twice. Rabbit polyclonal SOCS3-antibody (abcam, UK; 1:100 dilution) was added to the slides and incubated overnight at 4 °C. Detection of immunoreactivity and the subsequent steps of the immunohistochemistry protocol were performed as described for EGFR (see 5.3.2.1).

3.3.2.3 Protein expression analysis

Protein expression levels were semi-quantitatively assessed by a composite numerical score, based on the percentage of positively stained tumor cells multiplied by staining intensity, potentially ranging from 0 to 12. The percentage of labeled cells was scored as follows: 0 (no

or minimal reactivity, similar to non-neoplastic brain tissue), 1 (< 10 %), 2 (10 – 50 %), 3 (50 – 90 %) and 4 (> 90 %). Staining intensity was graded as 0 (negative), 1 (weak), 2 (moderate) or 3 (strong).

3.4 Statistical analyses

Fisher's exact test was used to assess frequency differences of *SOCS3* promoter hypermethylation between the different histological subtypes of gliomas (Figure 14b). In this regard we compared primary glioblastomas (pGB, n = 25) to other astrocytic gliomas (A + AA + sGB, n = 14), mixed oligoastrocytomas (OA + AOA, n = 11) and pure oligodenroglial neoplasms (O + OA, n = 10). P-values were verified for significance by employing Benjamini-Hochberg corrections for multiple testing.

Mann-Whitney U-test analyses were employed to compare *SOCS3* mRNA expression (Figure 14a), *EGFR* gene copy number (Figure 14c) and EGFR protein expression scores (Figure 14d) between tumors with and without *SOCS3* promoter hypermethylation.

In the cell-based functional assays two-sided student's t-test analyses were utilized to compare results between transfected and control cells (Figure 5). All statistical analyses were computed using the Graph Pad Prism Software (Version 5). The p-value of < 0.05 (*), < 0.01 (**) and < 0.001 (***) were considered as significant.

4 Results

4.1 Promoter methylation status of *SOCS3* in human gliomas

Previous experiments from our lab assessed the methylation status of the *SOCS3* promoter in a tumor panel consisting of 30 human gliomas and suggested that *SOCS3* promotor hypermethylation appeared preferentially in low-grade and anaplastic gliomas, while it was rare or absent in glioblastomas. This tumor panel contained the following histological glioma subtypes and grades as well as non-neoplastic brain tissues samples:

4 non neoplastic brain tissues (NB);

6 primary glioblastomas, WHO grade IV (*GB*);

4 anaplastic astrocytomas, WHO grade III (*AA*);

3 diffuse astrocytomas, WHO grade II (*A*);

6 anaplastic oligoastrocytomas, WHO grade III (*AOA*);

4 oligoastrocytomas, WHO grade II (*OA*);

7 anaplastic oligodendrogliomas, WHO grade III (*AO*);

and 3 oligodendrogliomas, WHO grade II (*O*).

To follow up on this observation in this doctoral thesis, the original tumor panel was expanded by analyzing *SOCS3* gene alterations in an additional set of 16 primary glioblastomas and 8 secondary glioblastomas, WHO grade IV (*GB*), as well as 6 non-neoplastic brain tissues by using direct sequencing analysis of sodium bisulfite modified DNA. Molecular genetic results of all tumors are shown in Figure 13.

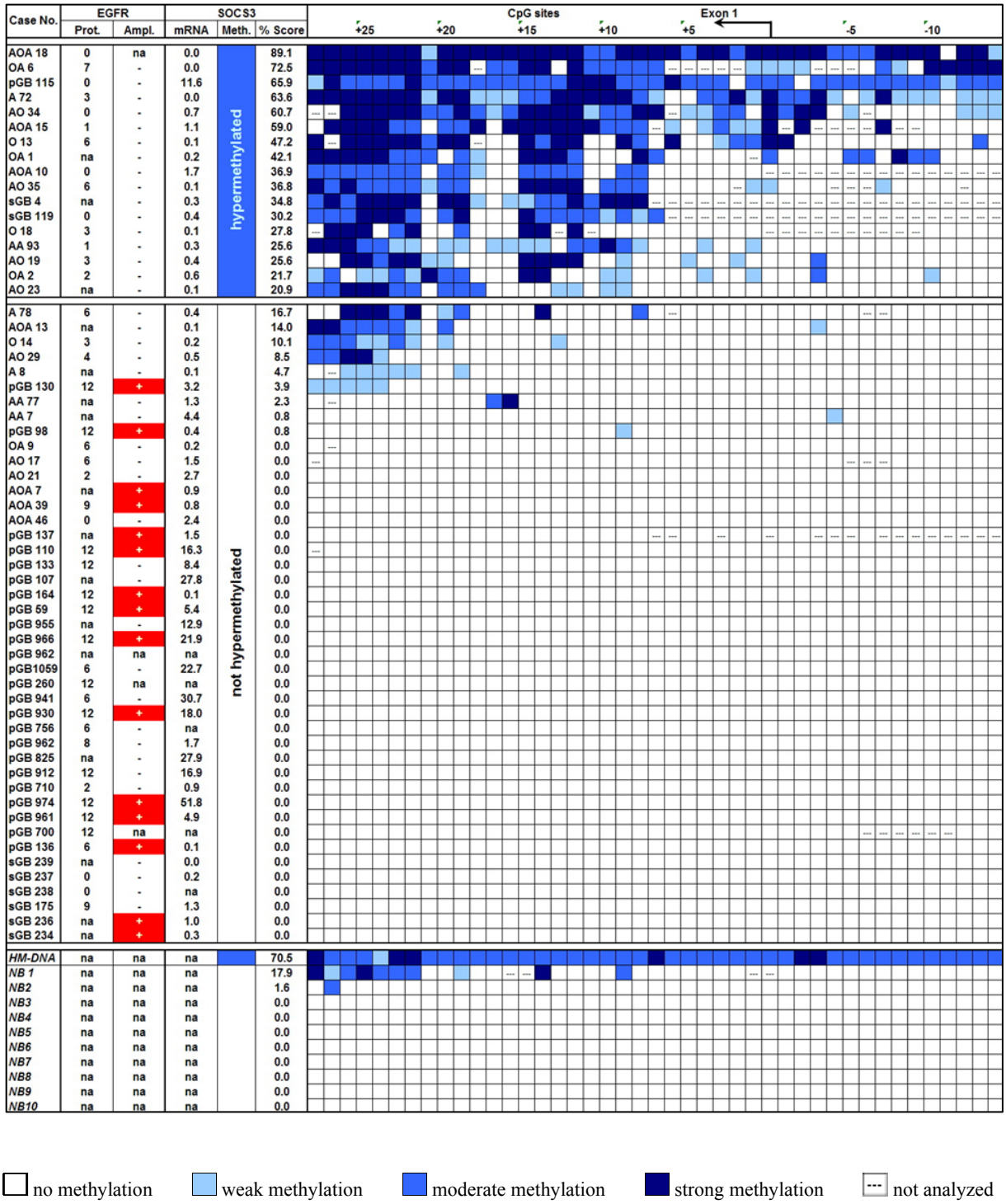

Figure 13: Synopsis of molecular aberrations of the *SOCS3* and the *EGFR* gene in human gliomas. *SOCS3* is frequently inactivated by promoter hypermethylation in a panel of 60 human gliomas. When analyzing the subgroup of primary glioblastomas, which is characterized by a high frequency of activating EGF receptor aberrations, *SOCS3* methylation is absent in nearly all samples. Only one primary glioblastoma (case no. *pGB* 115) showed

Figure 13: Synopsis of molecular aberrations of the *SOCS3* and the *EGFR* gene in human gliomas (continued). promoter hypermethylation of the *SOCS3* gene. Furthermore, *EGFR* amplification *(Ampl.,* gene copy number >5, here coloured in grey*)* is merely observed in tumors that lack *SOCS3* promoter hypermethylation. The *SOCS3* promoter methylation pattern has been assessed by direct bisulfite sequencing and shows each individual CpG site within the analyzed region spanning the transcription start site of *SOCS3*. (*% Score*, % *SOCS3* promoter methylation score). Additional information: EGFR protein expression level (EGFR *Prot*) as assessed by IHC; *SOCS3* mRNA expression level using real-time-(RT)-PCR.

4.1.1 Promoter hypermethylation and transcriptional downregulation of *SOCS3* in human gliomas

The *SOCS3* expression levels in the tumor panel were determined by real-time-(RT)-PCR. There was a significant inverse correlation between *SOCS3* promoter hypermethylation and *SOCS3* transcript levels (Mann-Whitney U-test, p=0.001). When comparing *SOCS3* mRNA expression levels according to the degree of promoter-methylation in the respective tumors, tumors with *SOCS3* hypermethylation (median: 0.3; interquartile range, IQR: 0.5) showed significantly lower *SOCS3* mRNA expression levels than those without promoter hypermethylation. This finding argues for a potential causal effect of *SOCS3* promoter hypermethylation concerning the decreased mRNA expression levels (Figure 14a).

4.1.2 *SOCS3* promotor hypermethylation is absent in primary glioblastomas

Next, the *SOCS3* methylation status was compared between the different glioma entities. When comparing the different glioma subtypes, *SOCS3* promoter hypermethylation -with a single exception (pGB115) - was absent in primary glioblastomas (1 out of 25 cases, 4 %). Furthermore, *SOCS3* promoter hypermethylation was significantly less frequent in primary glioblastomas compared to all other histological glioma subtypes, i.e. diffusely infiltrating astrocytic (A+AA+sGB: 4 out 14, 29 %; Fisher's exact test, p=0.047), mixed oligoastrocytic (OA+AOA: 6 out of 11, 55 %; p=0.001) and oligodendroglial (O+AO: 6 out of 10, 60 %; p=0.0008) neoplasms (Figure 14b).

4.2 *SOCS3* promoter hypermethylation is inversely correlated to *EGFR* gene dosage and EGFR protein expression

Primary glioblastomas usually comprise a high fraction of activating *EGFR* aberrations (Riemenschneider et al. 2010). When following up on the observation of a significantly less frequent *SOCS3* promoter hypermethylation in primary glioblastomas, the *EGFR* gene dosage was assessed by utilizing real-time PCR analysis. In addition, the EGFR protein expression levels were determined by using immunohistochemistry. These results were then correlated to the *SOCS3* promotor methylation status. A total of 15 tumors (2 secondary glioblastomas, 11 primary glioblastomas and 2 anaplastic oligoastrocytomas) showed a more than 5-fold increase of the *EGFR* gene dosage, consistent with *EGFR* amplification. None, of these tumors had a concomitant *SOCS3* promotor hypermethylation.
Statistical analysis corroborated this observation by revealing significantly lower *EGFR* gene copy numbers in tumors containing a methylated *SOCS3* promoter (median: 0.9; IQR: 0.4) than in tumors lacking this epigenetic aberration (median: 1.7; IQR: 19.0; Mann-Whitney U-test, p=0.0006; Figure 14c).

For assessing the EGFR protein status expression, EGFR protein levels between tumor samples with and without *SOCS3* promotor hypermethylation were determined semiquantitatively by means of immunohistochemistry.
When comparing the median EGFR protein score, it was significantly lower in tumors that exhibited *SOCS3* promoter hypermethylation (median: 1.5; IQR: 3.0) compared to tumors without (median: 8.5; IQR: 6.0) a methylated *SOCS3* promoter (Mann-Whitney U-test, p=0.0004; Figure 14d and 15). The single primary glioblastoma (pGB115) that exhibited *SOCS3* promoter hypermethylation did neither show a relevant increase in *EGFR* gene dosage (fold change: 1.2) nor expression of EGFR protein (Score: 0).
The SOCS3 staining – even after intense optimization efforts – did not reveal specific result and was thus not further evaluated.

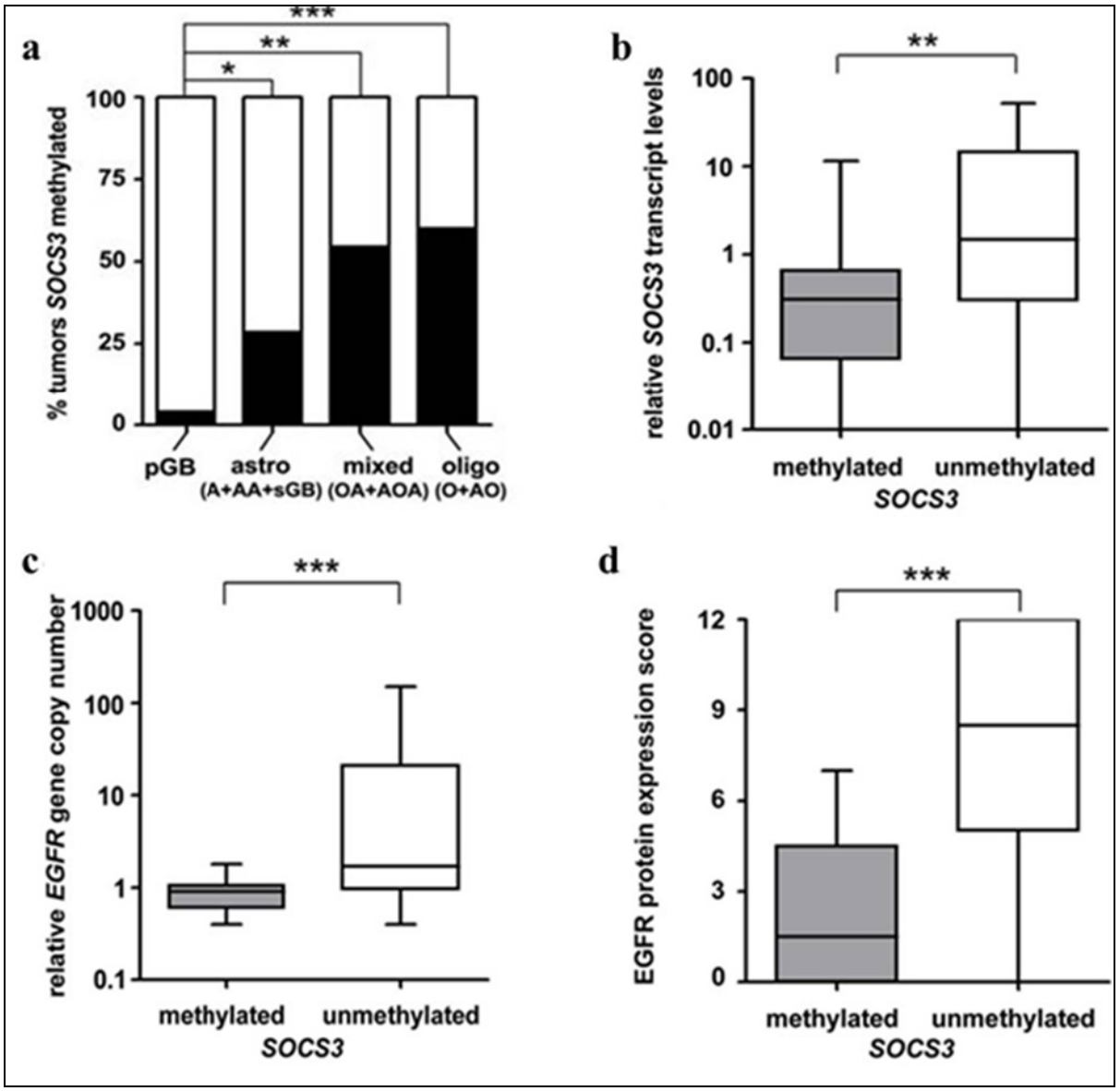

Figure 14: Statistical analysis of *SOCS3* promoter hypermethylation in human gliomas. **(a)** *SOCS3* promoter hypermethylation is significantly less frequent in pGB than in all other examined histological glioma subtypes astrocytic tumors, mixed oligoastrocytomas and oligodendrogliomas; (**b**) Tumor samples that show *SOCS3* promoter hypermethylation have significantly lower *SOCS3* transcript levels than tumors without *SOCS3* promoter hypermethylation. *SOCS3* promoter hypermethylation is significantly inversely correlated to EGFR aberrations. Both, the relative gene copy number of *EGFR* (**c**) as well as the protein expression score of EGFR (as assessed by IHC) (**d**) is significantly lower in tumors with *SOCS3* promoter hypermethylation than in patients lacking this molecular alteration.

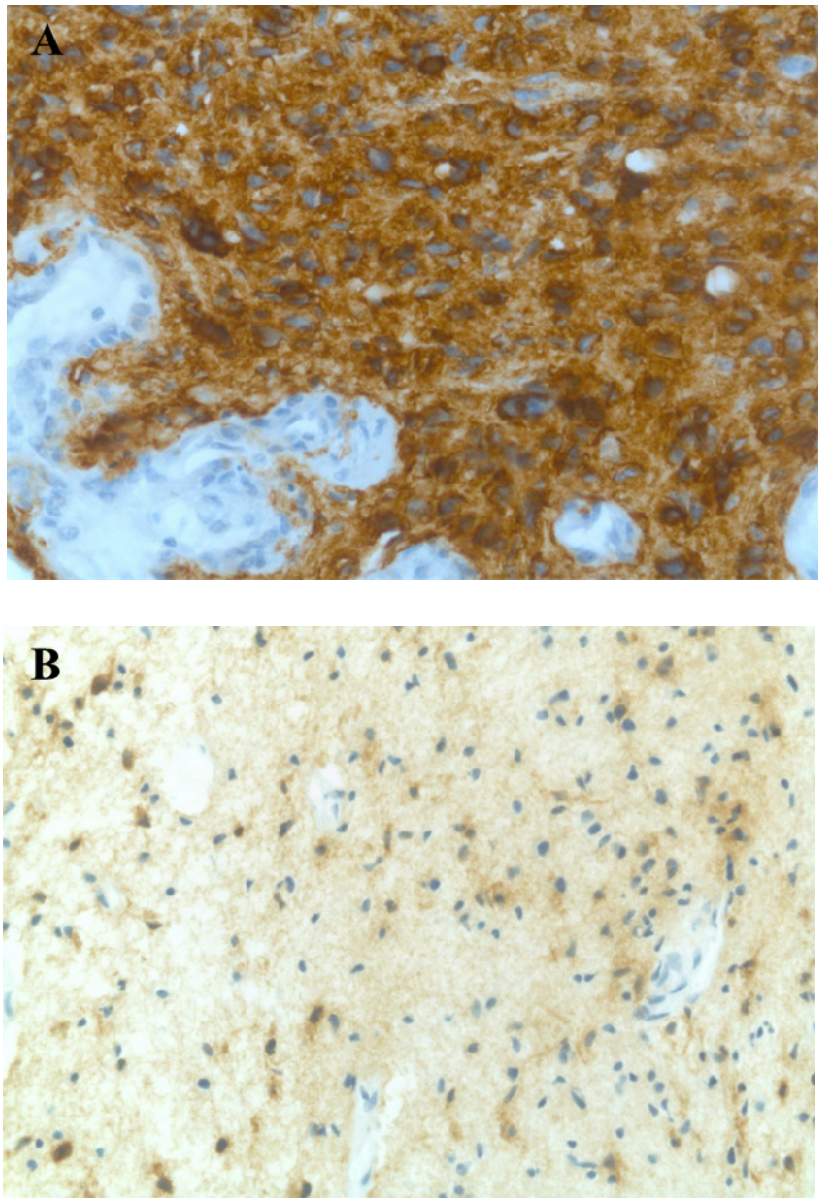

Figure 15: EGFR protein levels in two glioblastomas with different *SOCS3* methylation score and *EGFR* gene copy numbers.
(A) pGB130 showing a low *SOCS3* methylation score (5, 3.9 %), but high-level *EGFR* amplification (90.2x) and strong EGFR protein expression (score: 12). Nearly all tumor cells are intensively stained after using the anti-EGFR antibody (dilution 1:25; Dako, Hamburg); original microscopic magnification 400x. **(B)** A72 presenting a high *SOCS3* promoter methylation score (82, 63.6 %), but no *EGFR* amplification (0.4x) and low EGFR protein level (score: 3). Only a few tumor cells exhibit specific EGFR staining (anti-mouse EGFR antibody, dilution 1:25); original microscopic magnification 400x. Sections are counterstained with hemalum.

4.3 Mutational analysis of *SOCS3*

To exclude other potential alternative *SOCS3* inactivation mechanisms, such as mutations, an additional mutational analysis of the entire coding sequence (exon 2) of *SOCS3* was performed. This was done by utilizing SSCP/heteroduplex analysis (example pictured in Figure 16). PCR products from all 60 glioma samples were electrophoretically separated by using two different conditions (see Table 11, "Methods"). One single PCR sample product was sequenced because of aberrant band pattern within the SSCP analysis, but did not show any mutation. Analyzing the band patterns did not result in the detection of tumor-associated (somatic) mutations in any of the 60 glioma patients.

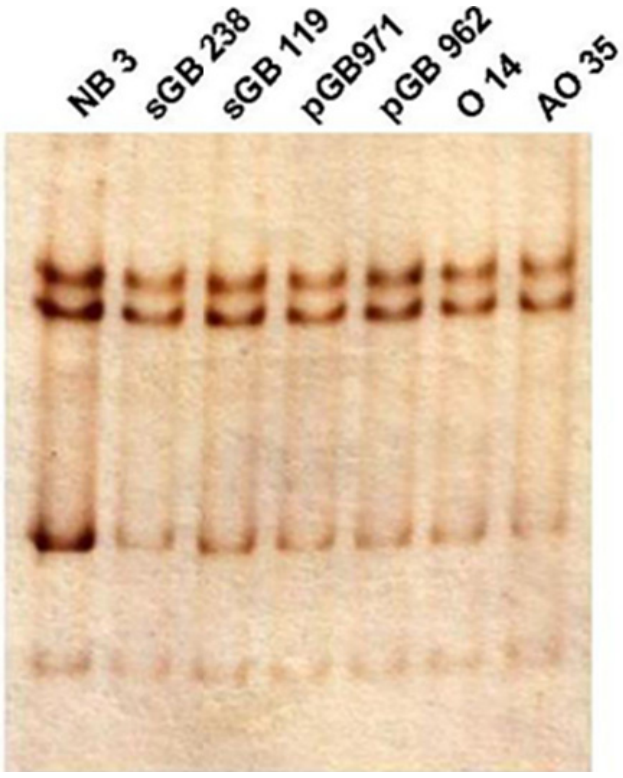

Figure 16: SSCP/heteroduplex analysis was performed to screen for mutations within the entire coding sequence (exon 2) of *SOCS3*. This SSCP gel (1 non-neoplastic brain tissue, 6 different gliomas) serves as an example for the band pattern results of 60 different gliomas and 4 non-neoplastic brain tissues. No tumor-associated (somatic) mutations were found in any of the 60 glioma samples. The depicted DNA samples were electrophoretically separated using the following conditions: *SOCS3* fragment 1, 10 % PAA/BAA, RT, 1:29.

4.4 *Knock-down* efficiency of *SOCS3* siRNAs

To analyze the functional characteristics of *SOCS3 depleted* glioblastoma cells *in-vitro*, two different siRNAs Hs_*SOCS3*_6 and custom siRNA_*SOCS3* (50 nM concentration; siRNA sequences are listed in Table 9, "Materials") were used to inhibit *SOCS3* transcription in A172, U251MG, TP365MG, U118MG, T98G and U87MG cell lines. In addition, All Stars Negative Control siRNA (Qiagen, Germany) was utilized to normalize for side-effects not being caused by specific siRNA inhibition.

All glioma cell lines were efficiently transfectable with nearly 95-100% of cells showing an uptake of fluorescently-labeled oligonucleotides (rhodamine dye). *Knock-down* efficiency (Figure 17) was determined using real-time (RT)-PCR and primers as described above.

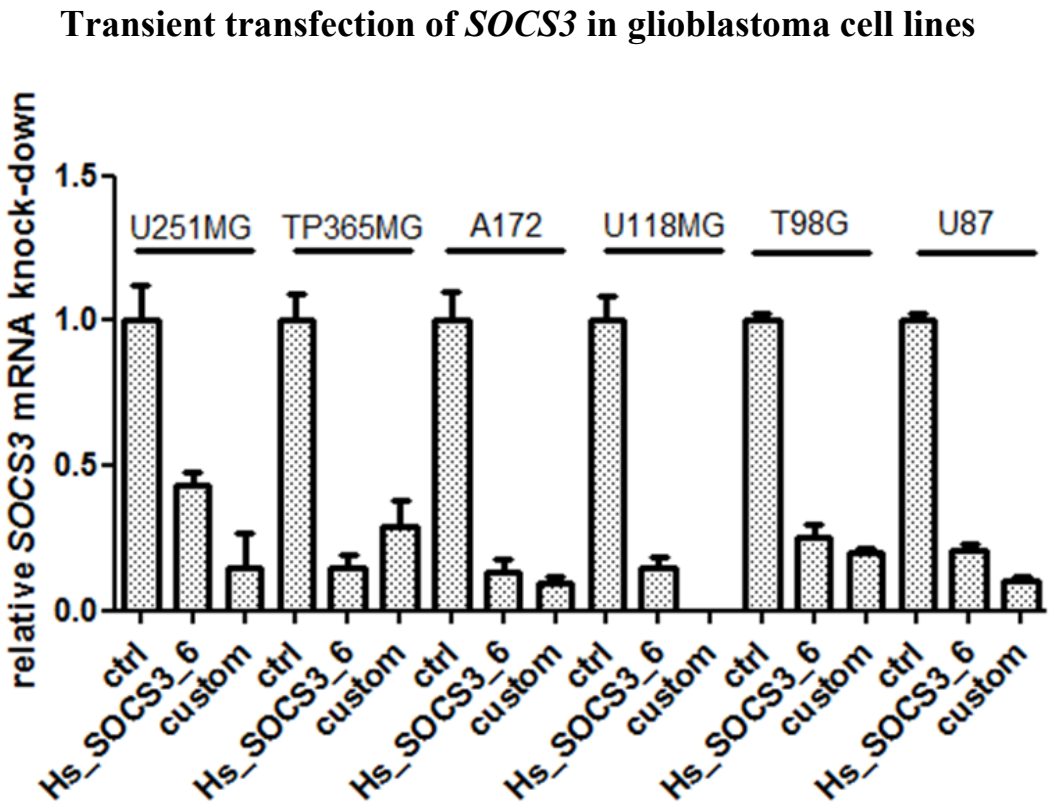

Figure 17: Transient transfection of *SOCS3* in glioblastoma cell lines. Note that compared to negative control cells (negative ctrl) all tested siRNAs (50 nM) caused markedly reduced *SOCS3* mRNA expression levels. Results were reproduced in at least three independent experiments (results are presented in means with standard deviation).

While transient transfection of siRNAs resulted in strong reduction of *SOCS3* mRNA levels, no decreased SOCS3 protein level could be detected. Using western blots with two different commercially available SOCS3 antibodies (Santa Cruz, #sc-73045 and Cell signaling, #2923), no reliable reduction of SOCS3 protein expression was observable. To exclude that this observation might be due to a prolonged half-life of the SOCS3 protein, stable-transfected U251MG, U87MG and A172 glioblastoma cell lines were generated. Again, no reliable reduction in SOCS3 protein levels could be observed. The absence of reduced protein expression on western blotting was thus assumed to be most likely due to cross reactivity or insufficient quality of the employed *SOCS3* antibodies.

4.5 Stable shRNA-mediated *knock-down* of *SOCS3* in U251MG glioblastoma cells

As outlined above, for further assessing the functional effects of *SOCS3* inactivation, vector-based shRNA-mediated RNAi was used to generate U251MG, U87MG and A172 glioblastoma cells with a stable *SOCS3 knock-down*. *SOCS3* mRNA expression was determined after this knockdown. Two different hairpins (sh1 and sh2) were used to avoid off-target effects of the respective shRNAs and two different subclones of each hairpin (sh1/2-1 and sh1/2-2) were utilized to exclude insertion-site specific side effects. Transfection with these two hairpins resulted in a relevant *SOCS3 knock-down* in comparison to the negative scrambled (scr) control. A subtotal reduction of *SOCS3* expression in U251MG glioblastoma cells transfected with hairpin 1 (86-99 %) and a somewhat lesser but relevant reduction of *SOCS3* expression in cells transfected with hairpin 2 (62-65 %) was accomplished (Figure 18).

SOCS3 mRNA expression reductions in U87MG and A172 glioma cells were much lower (hairpin 1: 55-62 %; for hairpin 2: <50 %). Therefore, these clones were not carried on for the following functional analysis.

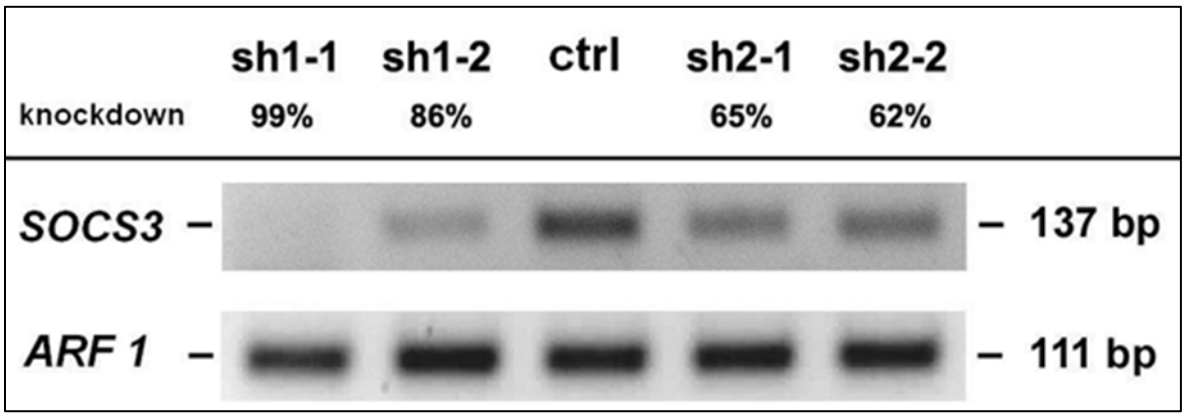

Figure 18: Generation of U251 glioblastoma cells with a stable shRNA-mediated *SOCS3 knock-down*. Two different hairpins (*sh1* and *sh2*) were utilized to exclude off-target effects of the respective shRNAs. For avoiding insertion-site specific side-effects we investigated two different subclones of each hairpin (*second digit within the respective denotation*). Note that in comparison to the scrambled negative control shRNA (*scr*) all four selected subclones demonstrate notably reduced *SOCS3* mRNA expression levels relative to the *ARF1* reference gene.

4.6 Investigation of the activation status of downstream targets within the EGFR signalling pathway after SOCS3 inactivation

Protein expression levels of glioblastoma cells were determined after SOCS3 *knock-down* in order to identify the activation, i.e. phosphorylation levels of EGFR-related downstream signaling pathway targets. Phosphorylation-specific antibodies were applied in western blot analyses against the following targets: MAPK (phosphorylated on Thr202/Tyr204), FAK (phosphorylated on Tyr397), STAT3 (phosphorylated on Tyr705), AKT (phosphorylated on Ser473).

When comparing SOCS3 *depleted* glioblastoma cells to the negative scrambled control cells, an activation of targets within the EGFR signalling pathway was observed. *SOCS3* depletion resulted in a strong and unequivocal increase in the phosphorylation levels of STAT3 and FAK in all investigated tumor cell subclones (relative to the respective negative control cells; Figure 19). The protein phosphorylation level of MAPK in dependence on *SOCS3* reduction was less consistent. An increased protein expression of p-MAPK was only detected in hairpin 1 and no increase, but a reduction of p-MAPK levels was detected in U251 glioblastoma cells transfected with hairpin 2. Protein phosphorylation levels of AKT did not show any relevant changes when comparing *SOCS3 knock-down* cells and control cells in their p-AKT expression pattern, which were fairly similar to that of the loading control α-Tubulin (Figure 19).

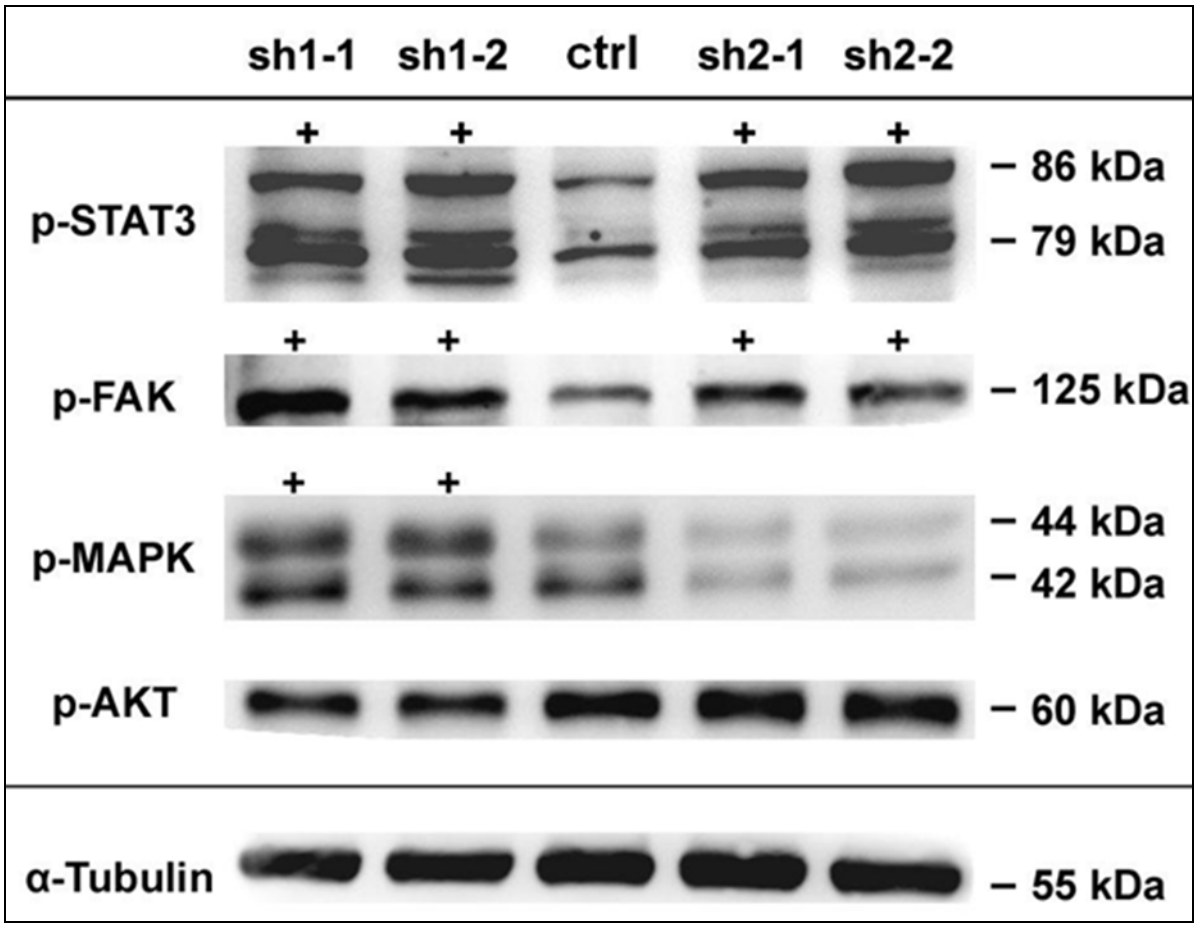

Figure 19: Western blot analysis for the activation of EGF receptor downstream signaling pathway members in U251MG *SOCS3 depleted* cells. Protein phosphorylation levels for both STAT3 and FAK are uniformly increased (+) in all four *SOCS3 knock-down* subclones in comparison to U251MG scrambled negative control cells (*scr*). The impact of *SOCS3 knock-down* on the activation levels of MAPK is equivocal showing an increase in protein phosphorylation (i.e. activation) only in hairpin 1 but not in hairpin 2 (*clones sh1-1 and sh1-2*). p-AKT protein expression levels appear completely unaffected by the inhibition of *SOCS3* expression in U251MG glioblastoma cells. α-Tubulin was used as a control to avoid unequal protein loading. Results were reproduced in at least three independent experiments.

4.7 Functional effects of *SOCS3 knock-down* in human glioblastoma cells

To investigate the functional consequences of *SOCS3 knock-down* in U251MG glioblastoma, cells cell-based assays for tumor cell proliferation, apoptosis and invasion were performed.

Tumor cell proliferation as investigated by BrdU incorporation assay (Roche, Germany) exhibited a heterogeneous either minor increase or reduction in individual *SOCS3 knock-down* subclones in comparison to the scrambled control cells but none of these changes emerged as statistically significant (Figure 20B).

By using the caspase-3/7 assay (Promega, Germany), a moderate inhibition of apoptotic activity in the majority (3 out of 4) of the investigated *SOCS3 knock-down* subclones was measurable. For two of the analyzed subclones (sh1-2 and sh2-2), statistically significant results were observed (students's t-test; sh1-2, p=0.0476; sh2-2, p=0.0001, Figure 20A).

Measuring the invasive characteristics of *SOCS3*-depleted U251MG glioblastoma cells in comparison to scrambled control cells revealed a predominant functional effect of *SOCS3* reduction on tumor cell invasion. Invasiveness was measured using a modified Matrigel^{TM}-coated Boyden chamber assay (BD Biosciences, San Jose, CA). All four investigated *SOCS3*-depleted tumor cell subclones showed an unequivocal increase in their invasive properties relative to the respective scrambled control cells. The highest increase (up to nearly 5-fold) was documented in subclone sh2-2. Using student's t-test analyses this increase proved highly significant in 3 out of the 4 analyzed *SOCS3 knock-down* subclones (sh1-1, p=0.005; sh2-1, p= 0.004; sh2-2, p=0.002; Figure 20C).

In conclusion, cell-based functional assays revealed the most obvious and strongest positive effect of *SOCS3* depletion on tumor cell invasion and a moderate negative impact on apoptosis, while tumor cell proliferation appeared unaffected.

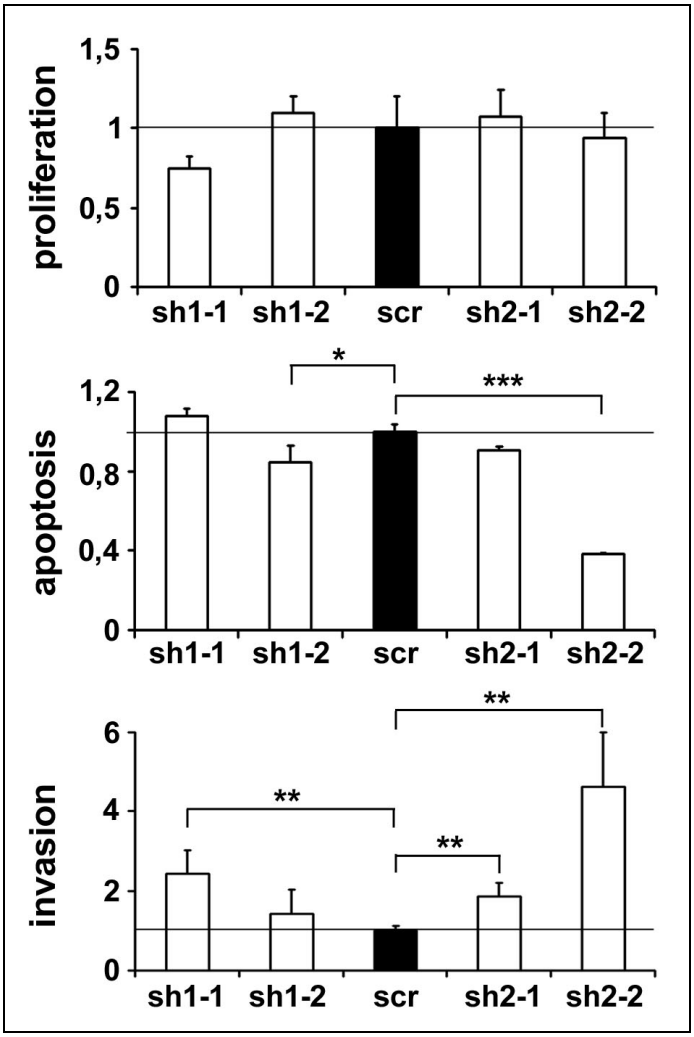

Figure 20: *In-vitro* effects of SOCS3 *knock-down* in U251MG glioblastoma cells
(A) To compare apoptotic activity a fluorometric caspase-3/-7 assay was used (Promega, Mannheim, Germany). **(B)** Proliferation was quantified using BrdU incorporation assay (Roche, Mannheim, Germany). **(C)** Cell invasion was assessed using modified Boyden-chamber transwell-assay with MatrigelTM coated membranes (24well; BD Biosciences, San Jose, CA). [The results of the *in-vitro* assays are shown in relative units setting the average result in the scrambled control cells to 1.0 (100%). Standard deviations are illustrated as error bars; asterisks indicate significant differences (*p-value* <0.05 (*), p-value <0.01 (**), p-value <0.001 (***). *scr:* scrambled negative cell control, *sh1-1 – sh2-2:* different SOCS3 *knock-down* sublones].

5 Discussion

SOCS3 acts as a negative regulator of the JAK/STAT signal transduction pathway and has been reported as a tumor suppressor in various human cancers. Up to date, the relevance of the *SOCS3* in diffusely infiltrating human gliomas was largely unknown. These tumors consist of a number of different subentities that are characterized by individual patterns of molecular aberrations (Louis et al. 2007).

Primary glioblastomas contain a high frequency of activating *EGFR* aberrations, while secondary glioblastomas and lower grade precursor lesions in their majority lack *EGFR* aberrations. They are instead characterized by frequent mutations in the *IDH1* and *TP53* genes as well as other molecular alterations (Ohgaki and Kleihues 2007, Balss et al. 2008).

In a preceding publication, Martini et al. (2008) reported on the negative prognostic effect of *SOCS3* promotor hypermethylation in glioblastoma patients. However, this study was restricted to primary glioblastomas and did not compare the SOCS3 methylation status with the individual patients´ EGFR gene status.

SOCS3 promotor hypermethylation in this doctoral thesis was identified as a novel player in the pathogenesis of gliomas that may substitutes for the absence of *EGFR* amplification in secondary glioblastomas, anaplastic and low-grade astrocytomas by activating identical downstream signaling pathways.

5.1 *SOCS3* inactivation by promoter hypermethylation in glioblastomas – an alternative mechanism to *EGFR* amplification and overexpression?

In this doctoral thesis, a panel of 60 human gliomas of different histological subtypes and WHO grades were investigated for *SOCS3* epigenetic alterations. With only a single exception (pGB115), *SOCS3* inactivation by promoter hypermethylation was absent in primary glioblastomas (4 %), i.e. in those types of tumors containing the highest rate of *EGFR* aberrations. Assessing the correlation between EGF receptor aberrations and *SOCS3* promoter hypermethylation in the tumor panel, it became clear that tumors with *SOCS3* promoter hypermethylation exhibited both - significantly lower relative *EGFR* gene copy numbers as well as significantly lower EGFR protein expression scores than tumors without this epigenetic aberration. This observation suggested that *SOCS3* inactivation by promoter hypermethylation might be an alternative molecular mechanism to *EGFR* amplification and overexpression in gliomas. Interestingly, two other recent publications provide further hints to this hypothesis, suggesting that there is an inverse relation between SOCS3 protein function and EGFR signaling. These publications reported on an influence of SOCS3 on the phosphorylation status of STAT3 (as also being a potential target in response to EGF) in human hepatocytes and in human embryonic kidney 293 cells (Seki et al. 2008, Xia et al. 2002), thus underlining that SOCS3 differentially regulates EGF receptor signaling.

This hypothesis is also in line with the fact that the single primary glioblastoma pGB115 in our panel that presented a hypermethylated *SOCS3* promotor neither showed increased *EGFR* gene copy numbers nor elevated EGFR protein expression. Reevaluation of this particular tumor's histology revealed that the tumor exhibited the classical morphological characteristics of glioblastoma and moleculary showed a wild-type genotype for *IDH1* and *IDH2* as typical for the majority of primary glioblastomas. As a consequence, these results do therefore not exclude that primary glioblastomas may bear a hypermethylated *SOCS3* promotor.

5.2 Low frequency of *SOCS3* hypermethylation in primary glioblastomas

Nevertheless, the low frequency of *SOCS3* promotor hypermethylation (4 %) in primary glioblastomas is different to the one described by Martini and colleagues in 2010, who reported on a hypermethylated *SOCS3* promoter in up to 35% of the primary glioblastomas. In the own tumor panel of 25 primary glioblastomas, there was an equal fraction of tumors with (13 cases) and without (12 cases) *EGFR* amplifications. The higher frequency of *SOCS3* promotor hypermethylation reported by Martini might be due to an overrepresentation of EGFR wild-type tumors in their used tumor panel. Maybe, these tumors are more susceptive to *SOCS3* promoter hypermethylation.

Closer to the own results showing low *SOCS3* methylation frequencies in primary glioblastomas, another study published by Zhou and colleagues (2007) did neither show *SOCS3* promoter hypermethylation nor a reduction in SOCS3 expression levels in 10 glioblastoma cell lines and 12 primary glioblastoma samples (Zhou et al. 2007).

5.3 SOCS3 *knock-down* leads to STAT3 and FAK activation

An activation of potential downstream signaling targets was assessed *in-vitro* by means of phosphorylation-specific antibodies and western blots in dependence on SOCS3 inactivation. For this, siRNA-mediated gene silencing was performed in a variety of established glioblastoma cell lines. In addition, stable transfections were performed with relevant *knock-down* efficiency in U251MG on the mRNA level (see Figure 18, Results). The fact that the own Western blot experiments did not present a reliable decrease of SOCS3 protein expression after transient or stable transfection might be well due to the fact that the used antibodies likely bind to other members of the SOCS protein family, which share high sequence homologies with SOCS3.

The investigation of the downstream signaling effects of SOCS3-depleted U251MG glioblastoma cells within the EGF receptor signaling pathway detected an intense and unequivocal increase in the phosphorylation levels of STAT3 and FAK in all analyzed SOCS3 *knock-down* clones in contrast to U251MG control cells. This positive effect of SOCS3 depletion on STAT3 activation is in line with the functional role of SOCS3 acting as a

negative regulator of JAK/STAT signaling (Cooney et al. 2002; Krebs and Hilton 2000). In addition, the observation of an increased FAK activation level after SOCS3 *knock-down* had been previously reported in human hepatocellular carcinoma cells and progenitor B lymphocytes (Le et al. 2007; Niwa et al. 2005). How exactly SOCS3 depletion increases FAK Y397 phosphorylation needs further investigation. Two studies report on two different phosphorylation possibilities. The first one by Niwa et al. (2005) reports that in human hepatocellular carcinoma there is a direct physical interaction of SOCS3 with phosphorylated FAK and this interaction then mediates polyubiquitination of FAK, resulting in proteasome-dependent degradation of FAK. The second paper by Le et al. (2007), points out that SOCS3 regulates CXCL12-induced FAK phosphorylation through the ubiquitin-proteasome pathway during B lymphopoiesis. STAT3 and FAK can also be phosphorylated by activated growth factor receptors, such as the epidermal growth factor receptor *(EGFR)*. For the sake of completeness, it should be mentioned that AKT *(proteinkinase B)* and MAPK *(mitogen-activated protein kinase, ERK1/2)* can also be phosphorylated by EGFR signaling.
These findings add further proof to the hypothesis that SOCS3 inactivation may function as an alternative mechanism for the activation of identical intracellular signaling pathways in those types of glioblastomas that do not bear activated EGF receptors.

By activation, i.e. phosphorylation, of STAT3, *SOCS3*-depleted cancer cells may affect diverse cellular functions, e.g. proliferation, apoptosis or migration and invasion (Imada and Leonard 2000; Yu et al. 2009).
The activation of FAK has been implemented to preferentially influence tumor cell growth, cytoskeletal and microtubule organization, and is thus functionally closely related to the invasive capacaties of different human cancers, including glioblastomas (Riemenschneider et al. 2005).
As two further downstream EGFR signaling intermediates, p44/p42 MAPK (mitogen-activated protein kinase, ERK1/2) and AKT (proteinkinase B), had been reported to be regulated by SOCS3 (Puhr et al. 2010, Senn et al. 2003, Yu et al. 2009), this study investigated the activation levels of these two proteins in dependence on SOCS3 in glioblastoma cells. In this project, investigation in U251MG globlastoma cells with a stable *SOCS3 knock-down* showed an unequivocal result for p42/p44 MAPK protein status, i.e. a

moderate increase in MAPK activation levels after transfection with only one of the two transfected hairpins directed against SOCS3 (sh1). This missing effect on MAPK activation for the second hairpin may be explained by the lesser SOCS3 *knock-down* efficiency of hairpin 2 (sh2) but may also argue for a less consistent impact of SOCS3 protein on the p44/p42 MAPK activation levels in glioblastoma cells. The phosphorylation status of AKT remained unaffected with no increase of AKT phosphorylation levels after SOCS3 *knock-down*. Taken together, these results do not support a close interrelationship between SOCS3 and AKT in human glioblastomas.

5.4 SOCS3 *knock-down* preferentially promotes tumor cell invasion

Following the observations obtained by Western blotting with phosphorylation-specific antibodies, the functional consequences resulting from SOCS3 inactivation in human glioblastoma cells were investigated. Thereby, a predominant effect on tumor cell invasion with uniformly and significantly increased invasiveness in *SOCS3*-depleted glioblastoma cells was observed. These findings are in line with results reporting on an increased migration and invasive potential after *SOCS3 knock-down* in other human tumors (Niwa et al. 2005; Puhr et al. 2009, Yang et al. 2008). In addition, the above described activation of STAT and FAK after *SOCS3 knock-down* is also consistent with a predominant functional *SOCS3* effect on tumor cell invasion.

Furthermore, an only moderate reduction of apoptotic cell properties was observed that, however, was statistically significant in two out of the four investigated *SOCS3 knock-down* clones. The only moderate and uneven effect of *SOCS3* reduction on apoptosis may be due to the circumstance that only the basal apoptosis rate was measured without any stimulation by apoptosis-inducing compounds. However, the detection of a significant deregulation in two subclones, each from different hairpins, argues against an off-target and for a true anti-apoptic effect of impaired *SOCS3* in glioma cells.

No consistent effects on tumor cell proliferation were observed after SOCS3 inactivation, arguing for negligible effect of *SOCS3* on tumor cell proliferation in glioblastoma cells.

Recapitulating the fact that more frequent *SOCS3* promoter hypermethylation and transcriptional downregulation was found in lower-grade astrocytic and oligodendroglial tumors than in glioblastomas and that these tumors share the diffuse infiltrative pattern but not

the high proliferative activity with glioblastomas, it is thus tempting to speculate that *SOCS3* inactivation in these gliomas may mainly substitute for the stimulating effect on tumor cell invasion but not on proliferation.

5.5 Conclusions

This study molecularly dissects the inactivation mechanisms of SOCS3 in different histological subtypes of human gliomas and functionally investigates the interrelationships of SOCS3 with EGF receptor signaling in glioblastomas.

Collectively, the own data demonstrate that *SOCS3* inactivation by promoter hypermethylation is significantly less frequent in primary glioblastomas than in the other investigated diffuse glioma entities and inversely related to *EGFR* amplification and overexpression (Figure 21). Functionally, SOCS3 silencing preferentially promotes glioblastoma cell invasion through STAT3 and FAK activation (Figure 21).

Potential follow-up experiments could be performed by transplantation of stably transfected *SOCS3 knock-down* and control cells in immunocompromized mice. Such experiments might bear the potential of establishing SOCS3 as a potential molecular target of therapy in gliomas.

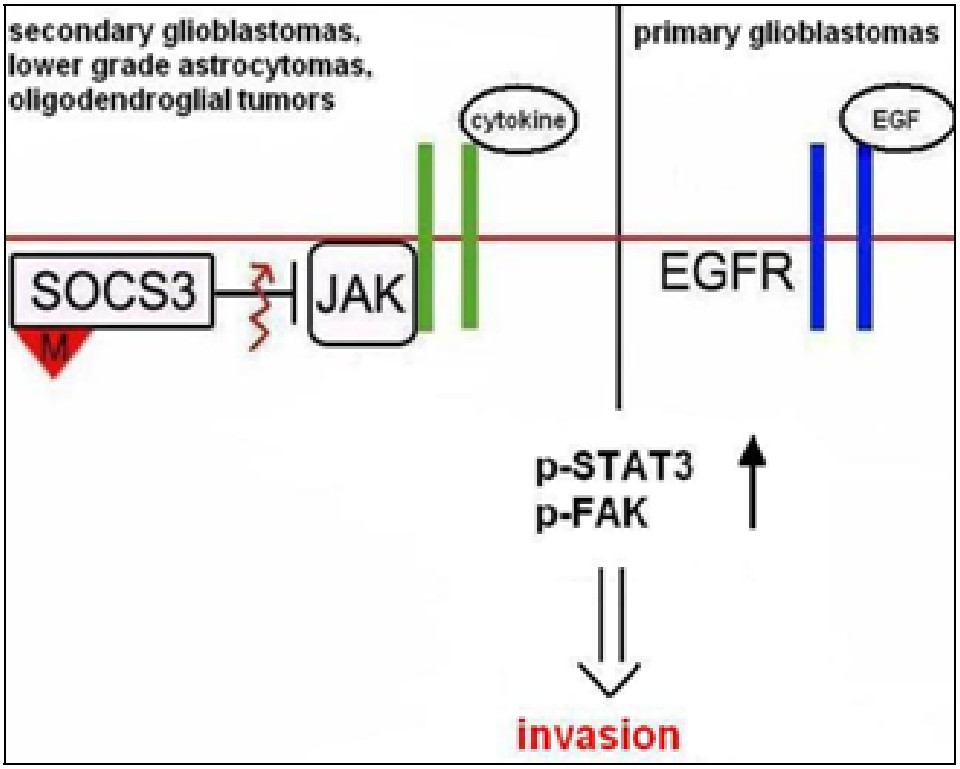

Figure 21: Model of SOCS3 function in gliomas. *SOCS3* inactivation by promotor hypermethylation (red-highlighted "M") substitutes for the stimulating effect of EGFR on invasion in secondary glioblastomas, lower grade astrocytomas and oligodendroglial tumors by STAT3 and FAK activation.

6 Abstract

The suppressor of cytokine signaling 3 *(SOCS3)* is one of eight structurally related genes of the SOCS gene family and has been suggested to function as a tumor suppressor by inhibition of the JAK/STAT signaling pathway. In the present doctoral thesis, 60 human gliomas of different histological types were investigated for *SOCS3* alterations and found to carry frequent *SOCS3* promoter hypermethylation and transcriptional downregulation. However, *SOCS3* promoter hypermethylation was virtually absent in primary glioblastomas, which are characterized by frequent epidermal growth factor receptor (EGFR) amplification and overexpression. Assessment of the relationship between *SOCS3* and *EGFR* aberrations revealed that *SOCS3* promoter hypermethylation was inversely related to both the *EGFR* gene dosage as well as the EGFR protein expression, thus suggesting *SOCS3* inactivation as a mechanism substituting for EGFR activation in a subset of gliomas. In support of this hypothesis, stable shRNA-mediated *SOCS3 knock-down* in U251 glioblastoma cells resulted in an activation of EGFR-related signaling pathways, i.e. an increase in the activation levels of STAT3, FAK and to a lesser extend MAPK, while the AKT phosphorylation levels remained unaffected. Functionally, *SOCS3*-depletion caused strongly increased tumor cell invasion with a moderate anti-apoptotic effect and no obvious impact on tumor cell proliferation. In summary, the findings summarized in this thesis suggest that *SOCS3* inactivation by promoter hypermethylation is mutually exlusive to EGFR activation in gliomas and preferentially promotes glioma cell invasion through STAT3 and FAK activation.

Prof. Dr. med. M. J. Riemenschneider

7 References

Aaronson DS, Horvath CM (2003) The JAK-STAT Pathway. Science STKE 197:cm11

Alexiou GA, Tsiouris S, Kyritsis AP, Polyzoidis KS, Fotopoulos AD (2007) The use of PET scan in glioblastoma multiforme. Journal of Neuro-Oncology 86:359-360

Balss J, Meyer J, Mueller W, Korshunov A, Hartmann C, von Deimling A (2008) Analysis of the IDH1 codon 132 mutation in brain tumors. Acta Neuropathol 116:597–602

Baltayiannis G, Baltayiannis N, Tsianos EV (2008) Suppressors of cytokine signaling as tumor repressors. Silencing of SOCS3 facilitates tumor formation and growth in lung and liver. J Buon. 13:263-265

Bondy ML, Scheurer ME, Malmer B, Barnholtz-Sloan JS, Davis FG, Il'yasova D, Kruchko C, McCarthy BJ, Rajaraman P, Schwartzbaum JA, Sadetzki S, Schlehofer B, Tihan T, Wiemels JL, Wrensch M, Buffler PA (2008) Brain tumor epidemiology: consensus from the Brain Tumor Epidemiology Consortium. Cancer 113:1953-68

Bradford MM (1976) A rapid and sensitive method for the quantitation of microgram quantities of protein utilizing the principle of protein-dye binding. Anal. Biochem 72:248-254

Cooney RN (2002) Suppressors of cytokine signaling (SOCS): inhibitors of the JAK/STAT pathway. Shock 17:83-90

Cotran RS, Robbins SL, Kumar V, Abbas (2004) Robbins and Cotran´s Pathologic Basis of Disease. Saunders 7th:1342-1344

Darnell Jr JE (2005) Validating Stat3 in cancer therapy. Nature Medicine 11:595-596

Dean BL, Drayer BP, Bird CR, Flom RA, Hodak JA, Coons SW, Carey RG (1990) Gliomas: classification with MR imaging. Radiology 174:411-5

Elliott J, Johnston JA (2004) SOCS: role in inflammation, allergy and homeostasis. Trends Immunol. 25:434-40

Farrell CJ, Plotkin SR (2007) Genetic causes of brain tumors: neurofibromatosis, tuberous sclerosis, von Hippel-Lindau, and other syndromes. Neurol Clin 25:925-946

Fleming TP, Saxena A, Clark WC, Robertson JT, Oldfield EH, Aaronson SA, Ali IU (1992) Amplification and/or Overexpression of Platelet-derived Growth Factor Receptors and Epidermal Growth Factor Receptor in Human Glial Tumors. Cancer Res 52:4550-4553

Fourouclas N, Li J, Gilby DC, Campbell PJ, Beer PA, Boyd EM, Goodeve AC, Bareford D, Harrison CN, Reilly JT, Green AR, Bench AJ (2008) Methylation of the suppressor of cytokine signaling 3 gene (SOCS3) in myeloproliferative disorders. Haematologica 93:1635-44

Frappaz D, Mornex F, Saint-Pierre G, Ranchere-Vince D, Jouvet A, Chassagne-Clement C, Thiesse P, Mere P, Deruty R (1999) Bone metastasis of glioblastoma multiforme confirmed by fine needle biopsy. Acta Neurochir 141:551-552

Friedman HS, McLendon RE, Kerby T, Dugan M, Bigner SH, Henry AJ, Ashley DM, Krischer J, Lovell S, Rasheed K, Marchev F, Seman AJ, Cokgor I, Rich J, Stewart E, Colvin OM, Provenzale JM, Bigner DD, Haglund MM, Friedman AH, Modrich PL (1998) DNA mismatch repair and O6-alkylguanine-DNA alkyltransferase analysis and response to Temodal in newly diagnosed malignant glioma. J Clin Oncol 16:3851–7

Frommer M, McDonald LE, Millar DS, Collis CM, Watt F, Grigg GW, Molloy PL, Paul CL (1992) A genomic sequencing protocol that yields a positive display of 5-methylcytosine residues in individual DNA strands. Proc Natl Acad Sci USA 89(5):1827-31

Hansen JA, Lindberg K, Hilton DJ, Nielsen JH, Billestrup N (1999) Mechanism of Inhibition of Growth Hormone Receptor Signaling by Suppressor of Cytokine Signaling Proteins. Mol. Endocrinol. 13:1832-1843

He B, You L, Uematsu K, Zang K, Xu Z, Lee AY (2003) SOCS-3 is frequently silenced by hypermethylation and suppresses cell growth in human lung cancer. Proc Natl Acad Sci USA100:14133-8

Hegi ME, Diserens AC, Gorlia T, Hamou MF, de Tribolet N, Weller M, Kros JM, Hainfellner JA, Mason W, Mariani L, Bromberg JE, Hau P, Mirimanoff RO, Cairncross JG, Janzer RC, Stupp R (2005) MGMT Gene Silencing and Benefit from Temozolomid in Glioblastoma. N. Engl. J. Med. 352:997–1003

Ichimura K, Bondesson Bolin M, Goike HM, Schmidt EE, Moshref A, Collins VP (2000) Deregulation of the $p14^{ARF}$/MDM2/p53 Pathway is a Prerequisite for Human Astrocytic Gliomas with G_1-S Transition Control Gene Abnormalities. Cancer Res 60:417

Ichimura K, Schmidt EE, Goike HM, Collins VP (1996) Human glioblastomas with no alterations of the CDKN2A (p16INK4A, MTS1) and CDK4 genes have frequent mutations of the retinoblastoma gene. Oncogene 13(5):1065-72

Imada K, Leonard WJ (2000) The Jak-STAT pathway. Mol Immunol. 37:1-11

Kamura T, Sato S, Haque D, Liu L, Kaelin WG Jr, Conaway RC, Conaway JW (1998) The Elongin BC complex interacts with the conserved SOCS-box motif present in members of the SOCS, ras, WD-40 repeat, and ankyrin repeat families.Genes Dev. 12:3872-81

Kieffer SA, Salibi NA, Kim RC, Lee SH, Cacayorin ED, Modesti LM (1982) Multifocal glioblastoma: diagnostic implications. Radiology 143:709-710

Kleihues P, Burger PC, Collins VP, Newcomb EW, Ohgaki H, Cavenee WK (2007) Glioblastoma. In WHO-Classification of Tumors. Pathology and Genetics. Tumors of the Nervous System, Kleihues P, Canenee WK (Herausgeber), IARC Press, Lyon, pp. 29-3

Kleihues P, Kiessling M, Wiestler. Tumoren des Nervensystems. In Böcker W, Denk H, Heitz PhU (Herausgeber) Pathologie, 3. Auflage, Urban &Fischer 2003, S. 318-321

Kleihues P, Ohgaki H (1999) Primary and secondary glioblastomas: from concept to clinical diagnosis. Neuro-oncol. 1:44-51

Komyod W, Bohm M, Metze D, Heinrich PC, Behrmann I (2007) Constitutive suppressor of cytokine signaling 3 expression in confers a growth advantage to a human melanoma cell line. Mol Cancer Res 5:271-8

Krebs DJ, Hilton DJ (2000) SOCS: physiological suppressors of cytokine signaling. J Cell Sci. 113 (Pt 16):2813-9

Kunitz A,Wolter M,Van Den Boom J, Felsberg J, Tews B, Hahn M, Benner A, Sabel M, Lichter P, Reifenberger G, Von Deimling A, Hartmann C (2007) DNA hypermethylation and Aberrant Expression of the EMP3 Gene at 19q13.3 in Human Gliomas. Brain Pathology, Volume 17, 4:363–370

Lacroix M, Abi-Said D, Fourney DR, Gokaslan ZL, Shi W, DeMonte F, Lang FF, McCutcheon IE, Hassenbusch SJ, Holland E, Hess K, Michael C, Miller D, Sawaya R (2001) A multivariate analysis of 416 patients with glioblastoma multiforme: prognosis, extent of resection, and survival, J Neurosurg 95:190–98

Lahkola A, Auvinen A, Raitanen J, Schoemaker MJ, Christensen HC, Feychting M, Johansen C, Klæboe L, Lönn S, Swerdlow AJ, Tynes T, Salminen T (2007) Mobile phone use and risk of glioma in 5 North European countries. International Journal of Cancer, 120:1769–1775

Latchaw RE, editor (1991) MR and CT imaging of the head, neck and spine. In: Mosby Yearbook. St. Louis 449-471.

Le Y, Zhu BM, Harley B, Park SY, Kobayashi T, Manis JP, Luo HR, Yoshimura A, Hennighausen L, Silberstein LE (2007) SOCS3 protein developmentally regulates the chemokine receptor CXCR4-FAK signaling pathway during B lymphopoiesis. Immunity 27:811-823

Livak KJ, Schmittgen TD (2001) Analysis of relative gene expression data using *Real-time* quantitative PCR and the 2(-Delta Delta C(T)) Method. Methods 25:402-8

Lönn S, Ahlbom A, Hall P, Feychting M and the Swedish Interphone Study Group (2005) Long-Term Mobile Phone Use and Brain Tumor Risk. Am. J. Epidemiol. 161: 526-535

Louis DN, Ohgaki H, Wiestler OD, Cavenee WK (2007) WHO Classification of Tumours of the Central Nervous System. Fourth Edition. World Health Organization, Lyon

Marine JC, McKay C, Wang D, Topham DJ, Parganas E, Nakajima H, Pendeville H, Yasukawa H, Sasaki A, Yoshimura A, Ihle JN (1999) SOCS3 is essential in the regulation of fetal liver erythropoiesis. Cell 98:617-2714

Martini M, Pallini R, Luongo G, Cenci T, Lucantoni C, Larocca LM (2008) Prognostic relevance of SOCS3 hypermethylation in patients with glioblastoma multiforme. Int J Cancer 123:2955-60

Maxam AM, Gilbert W (1980) Sequencing end-labeled DNA with base-specific chemical cleavages. Methods Enzymol 65:499-560

Mueller W, Nutt CL, Ehrich M, Riemenschneider MJ, von Deimling A, van den Boom D, Louis DN (2007) Downregulation of RUNX3 and TES by hypermethylation in glioblastoma. Oncogene 26:583-93

Nakamura M, Watanabe T, Klangby U, Asker C, Wiman K, Yonekawa Y, Kleihues P, Ohgaki H (2001) $p14^{ARF}$ Deletion and Methylation in Genetic Pathways to Glioblastomas. Brain Pathology 11(2):159–168

Nicholson SE, Willson TA, Farley A, Starr R, Zhang JG, Baca M, Alexander WS, Metcalf D, Hilton DJ, Nicola NA (1999) The Mutational analyses of the SOCS proteins suggest a dual domain requirement but distinct mechanisms for inhibition of LIF and IL-6 signal transduction. EMBO Journal 18:375–385

Nishizaki T, Ozaki S, Harada K, Ito H, Arai H, Beppu T, Sasaki K (1998) Investigation of genetic alterations associated with the grade of astrocytic tumor by comparative genomic hybridization. Genes Chromosomes Cancer 21:340-6

Niwa Y, Kanda H, Shikauchi Y, Saiura A, Matsubara K, Kitagawa T, Yamamoto J, Kubo T, Yoshikawa H (2005) Methylation silencing of SOCS-3 promotes cell growth and migration by enhancing JAK/STAT and FAK signalings in human hepatocellular carcinoma. Oncogene 24:6406-6417

Noonan JP, Grimwood J, Schmutz J, Dickson M, Myers RM (2004) Gene Conversion and the Evolution of Protocadherin Gene Cluster Diversity. Genome Res. 14:354-366

Ohgaki H, Kleihues P (2005) Epidemiology and etiology of gliomas. Acta Neuropathol. 109:93-108
Ohgaki H, Kleihues P (2007) Genetic pathways to primary and secondary glioblastoma. Am J Pathol. 170:1445-53

Orita M, Iwahana H, Kanazawa H, Hayashi K, Sekiya T (1989) Detection of polymorphisms of human DNA by gel electrophoresis as single-strand conformation polymorphisms. Proc Natl Acad Sci U S A 86:2766-2770

O'Shea JJ, Pesu M, Borie DC, Changelian PS (2004) A new modality for immunosuppression: targeting the JAK/STAT pathway. Nature Reviews Drug Discovery 3:555-564

Parsons DW, Jones S, Zhang S, Cheng-Ho Lin J, Leary RJ, Angenendt P, Mankoo P, Carter H, Siu IM, Gallia GL, Olivi A, McLendon R, Rasheed BA, Keir S, Nikolskaya T, Nikolsky Y, Busam DA, Tekleab H, Diaz LA, Hartigan J, Smith DR, Strausberg RL, Kazue S, Marie N, Shinjo SMO, Yan H, Riggins GJ, Bigner DD, Karchin R, Papadopoulos N, Parmigiani G, Vogelstein B, Velculescu VE, Kinzler KW (2008) An Integrated Genomic Analysis of Human Glioblastoma Multiforme. Science 321:1807

Pasquier B, Pasquier D, N'Golet A, Panh MH, Couderc P (1980) Extraneural metastases of astrocytomas and glioblastomas: clinicopathological study of two cases and review of literature. Cancer 45:112-25

Piessevaux J, Lavens D, Peelman F, Tavernier J (2008) The many faces of the SOCS box. Cytokine Growth Factor Rev.19:371-81

Puhr M, Santer FR, Neuwirt H, Marcias G, Hobisch A, Culig Z (2010) SOCS-3 antagonises the proliferative and migratory effects of fibroblast growth factor-2 in prostate cancer by inhibition of p44/p42 MAPK signalling. Endocr Relat Cancer 17:525-38

Puhr M, Santer FR, Neuwirt H, Marcias G, Hobisch A, Culig Z (2009) Down-regulation of suppressor of cytokine signaling-3 causes prostate cancer cell death through activation of the extrinsic and intrinsic apoptosis pathways. Cancer Res. 69:7375-84

Quesnelle KM, Boehm AL, Grandis JR (2007) STAT-mediated EGFR signaling in cancer. J Cell Biochem. 102:311-9

Reed AS, Unger EK, Olofsson LE, Piper ML, Myers MG Jr, Xu AW (2010) Functional role of suppressor of cytokine signaling 3 upregulation in hypothalamic leptin resistance and long-term energy homeostasis. Diabetes 59:894-906

Reifenberger G, Collins VP (2004) Pathology and molecular genetics of astrocytic gliomas. J Mol Med. 82:656-70

Riemenschneider MJ, Mueller W, Betensky RA, Mohapatra G, Louis DN (2005) In situ analysis of integrin and growth factor receptor signaling pathways in human glioblastomas suggests overlapping relationships with focal adhesion kinase activation. Am J Pathol. 167:1379-87

Riemenschneider MJ, Betensky RA, Pasedag SM, Louis DN (2006) AKT activation in human glioblastomas enhances proliferation via TSC2 and S6kinase signaling. Cancer Res. 66:5618-23

Riemenschneider MJ, Reifenberger G (2009) Molecular Neuropathology of Gliomas. Review. Int. J. Mol. Sci. 10:184-212

Riemenschneider MJ, Reifenberger G (2009) Astrocytic tumors. Recent Results Cancer Research 171:3–24

Riemenschneider MJ, Jeuken JW, Wesseling P, Reifenberger G (2010) Molecular diagnostics of gliomas: state of the art. Acta Neuropathol 120:567-584

Sanger F, Nicklen S, Coulson AR (1977) DNA sequencing with chain-terminating inhibitors. Proc Natl Acad Sci USA 74:5463-7

Sasi W, Jiang WG, Sharma A, Mokbel K (2010) Higher expression levels of SOCS 1,3,4,7 are associated with earlier tumor stage and better clinical outcome in human breast cancer. BMC Cancer 10:178

Schiffer D, Dohrmann GJ, Farwell JR, Flannery JT (1976) Brain Tumors. Biology, Pathology and Clinical References. J Neurosurg. 44:442-8

Schröck E, Blume C, Meffert M-C, du Manoir S, Bersch W, Kiessling M, Lozanowa T, Thiel G,Witkowski R, Ried T, Cremer T (1996) Recurrent gain of chromosome arm 7q in low-grade astrocytic tumors studied by comparative genomic hybridization. Genes, Chromosomes and Cancer 15:199–205

Shirai K, Siedow MR, Chakravarti A (2011) Antiangiogenic therapy for patients with recurrent and newly diagnosed malignant gliomas. Epub J Oncol.

Stupp R, Mason WP, van den Bent MJ, Weller M, Fisher B, Taphoorn MJ, Belanger K, Brandes AA, Marosi C, Bogdahn U, Curschmann J, Janzer RC, Ludwin SK, Gorlia T, Allgeier A, Lacombe D, Cairncross JG, Eisenhauer E, Mirimanoff RO (2005) Radiotherapy plus Concomitant and adjuvant Temozolomid for Glioblastoma. N. Engl. J. Med. 352:987–996

Sutherland KD, Lindeman GJ, Choong DY, Wittlin S, Brentzell L, Phillips W, Campbell IG, Visvader JE (2004) Differential hypermethylation of SOCS genes in ovarian and breast carcinomas. Oncogene 23:7726-33

Tepel M, Roerig P, Wolter M, Gutmann DH, Perry A, Reifenberger G, Riemenschneider MJ (2008) Frequent promoter hypermethylation and transcriptional downregulation of the NDRG2 gene at 14q11.2 in primary glioblastoma. Int J Cancer 123:2080-6

Tokita T, Maesawa C, Kimura T, Kotani K, Takahashi K, Akasaka T, Masuda T (2007) Methylation status of the SOCS3 gene in human malignant melanomas. Int J Oncol. 30:689-94

van den Boom J, Wolter M, Kuick R, Misek DE, Youkilis AS, Wechsler DS, Sommer C, Reifenberger G, Hanash SM (2003) Characterization of gene expression profiles associated with glioma progression using oligonucleotide-based microarray analysis and *Real-time* reverse transcription-polymerase chain reaction. Am J Pathol. 163:1033-43

Waha A, Güntner S, Huang T H-M, Yan P.S, Arslan B, Pietsch T, Wiestler OD (2005) Epigenetic silencing of the protocadherin family member pcdh-gamma-A11 in astrocytomas. Neoplasia 7:193–199

Watanabe T, Katayama Y, Yoshino AD, Yachi K, Ohta T, Ogino A, Komine C, Fukushima T (2007) Abberant hypermethylation of p14ARF and O6-methylguanine-DNA methyltransferase genes in astrocytoma progression. Brain Pathology 17:5-10

Weber A, Hengge UR, Bardenheuer W, Tischoff I, Sommerer F, Markwarth A, Dietz A, Wittekind C and Tannapfel A (2005) SOCS-3 is frequently methylated in head and neck squamous cell carcinoma and its precursor lesions and causes growth inhibition. Oncogene 24:6699-6708

Westphal M (2003) Epidemiologie und Ätiopathogenese. In Schlegel U, Weller M, Westphal M (Herausgeber). Neuroonkologie, 2. Auflage, Thieme, 2-10

Wong AJ, Bigner SH, Bigner DD, Kinzler KW, Hamilton SR, Vogelstein B (1987) Increased expression of the epidermal growth factor receptor gene in malignant gliomas is invariably associated with gene amplification. Proc Natl Acad Sci USA 84:6899–6903

Xia L, Wang L, Chung AS, Ivanov SS, Ling MY, Dragoi AM, Platt A, Gilmer TM, Fu XY and Chin YE (2002) Identification of both positive and negative domains within the epidermal growth factor receptor COOH-terminal region for signal transducer and activator of transcription (STAT) activation. J Biol Chem 277:30716-30723

Yang SF, Yeh YT, Wang SN, Hung SC, Chen WT, Huang CH and Chai CY (2008) SOCS-3 is associated with vascular invasion and overall survival in hepatocellular carcinoma. Pathology 40:558-563

Ying M, Li D, Yang L, Wang M, Wang N, Chen Y, He M and Wang Y (2010) Loss of SOCS3 expression is associated with an increased risk of recurrent disease in breast carcinoma. J Cancer Res Clin Oncol 136:1617-1626

Yu H, Pardoll D and Jove R (2009) STATs in cancer inflammation and immunity: a leading role for STAT3. Nat Rev Cancer 9:798-809

Zhou H, Miki R, Eeva M, Fike FM, Seligson D, Yang L, Yoshimura A, Teitell MA, Jamieson CA and Cacalano NA (2007) Reciprocal regulation of SOCS 1 and SOCS3 enhances resistance to ionizing radiation in glioblastoma multiforme. Clin Cancer Res 13:2344-2353

8 Acknowledgements

Mein erster Dank gilt meinem Doktorvater Herrn Prof. Dr. med. M. J. Riemenschneider für die Überlassung der sehr interessanten und methodisch vielseitigen Aufgabenstellung, der Anleitung zum wissenschaftlichen Arbeiten, dem Korrekturlesen meiner Arbeit und die exzellente Betreuung.

Mein weiterer großer Dank gebührt Herrn Prof. Dr. med. G. Reifenberger für die Möglichkeit, meine Promotion am Institut für Neuropathologie der Heinrich-Heine-Universität Düsseldorf durchführen zu können. Zudem möchte ich Ihm für seine wertvollen Anregungen zum Finalisieren dieses Projekts danken.
Bei Herrn Prof. Dr. med. R. Haas bedanke ich mich besonders für die freundliche Übernahme und Erstellung des Korreferats.

Nadine Lottmann und Fr. Dr. rer. nat. Natalie Schmidt aus der neuroonkologischen Arbeitsgruppe des Instituts für Neuropathologie Düsseldorf gilt mein besonderer Dank. Sie haben mich bei meiner praktischen Arbeit im Labor sehr unterstützt. Ihr Wissen und ihre Ideen waren mir immer eine große Hilfe. Zudem standen sie mir jederzeit mit unerschöpflichem Einsatz und bewundernswerter Ausdauer für Fragen und Probleme jeglicher Art (!) zur Verfügung.

Franziska Liesenberg möchte ich für ihre unermüdliche Hilfe bei der Durchführung der Methylierungsanalysen und ihre emotionale Unterstützung während der gesamten Dissertationszeit danken.
Bei allen nicht persönlich genannten Mitarbeitern des Instituts für Neuropathologie Düsseldorf bedanke ich mich für die Hilfe und für das überaus angenehme Arbeitsklima.

Mein herzlicher Dank gilt meinen Eltern für Ihre liebevolle Fürsorge, ihr Verständnis und Ihre grenzenlose Unterstützung in meiner gesamten Ausbildung.
Dir, mein lieber Friedrich, danke ich von ganzem Herzen für Deine beständige Geduld, Deinen Beistand und Deine Ermutigung zum Voranbringen dieser Arbeit.

9 Abbreviations

A	diffuse astrocytoma, WHO grade II
AA	anaplastic astrocytoma, WHO grade III
AO	anaplastic oligodendroglioma, WHO grade III
AOA	anaplastic oligoastrocytoma, WHO grade III
APS	ammoniumpersulfat
bp	base pairs
BrdU	Bromodeoxyuridine
BSA	bovine serum albumin
°C	degree Celsius
cDNA	copy deoxyribonucleic acid
CpG	Cytosin-phosphatidyl-Guanin
DAPI	4',6-Diamidino-2-Phenylindole
DMEM	Dulbecco's modification Eagle's medium
DMSO	dimethylsulfoxid
DNA	deoxyribonucleic acid
dNTP	desoxyribonucleoside-5.-triphosphat
ds-	(prefix) double-stranded
DTT	dithiothreitol
EDTA	ethylendiamintetraacetat
EGFR	Epidermal-Growth-Factor-Receptor
FCS	fetal calf serum
for	forward
GB	glioblastoma, WHO grade IV
GFP	green fluorescent protein
h	hour
JAK	Janus Kinase
kDa	kilodaltons
MRI	magnetic resonance imaging
mA	milli-ampere

min	minute
ml	milliliter
mRNA	messenger ribonucleic acid
NB	on-neoplastic brain tissue
µl	microliter
OA	diffuse oligoastrocytoma, WHO grade II
pGB	primary glioblastoma, WHO grade IV
PAGE	polyacrylamide gel electrophoresis
PBS	phosphate-buffered saline
PCR	polymerase chain reaction
rev	reverse
RNA	ribonucleic acid
RNAi	RNA interference
RNase	ribonuclease
rpm	rounds per minute
RT	room temperature
RT-PCR	reverse transcription polymerase chain reaction
SD	standard deviation
SDS	sodium dodecyl sulfate
sec	second
sGB	secondary glioblastoma, WHO grade IV
shRNA	small hairpin RNA
siRNA	small interfering RNA
SOCS	Suppressor of cytokine signaling
SSCP	Single strand conformation polymorphism
STAT	Signal Transducer and Activator of Transcription
Taq	Thermus aquaticus
TBE	Tris-borate-EDTA
TBS-T	Tris-buffered saline with Tween 20
TE	Tris-EDTA
TEMED	N-N-N-N-Tetraethylmethyldiamine

Tris	Tris(hydroxymethyl)aminomethane
U	unit
V	voltage
W	watt
WHO	World Health Organization

All genes, proteins and transcripts that are used here are abbreviated according to the National Center for Biotechnology Information (NCBI) GenBank short forms of the gene names (free online access is available via http://www.ncbi.nlm.nih.gov/).

10 Eidesstattliche Versicherung

Ich versichere an Eides statt, dass die Dissertation selbstständig und ohne unzulässige fremde Hilfe erstellt worden ist und die hier vorgelegte Dissertation nicht von einer anderen Medizinischen Fakultät abgelehnt worden ist.

21.05.2012, Carina Lindemann

11 Supplement

Die Ergebnisse der vorliegenden Dissertation wurden als Vortrag auf folgenden Kongressen vorgestellt:

1. Carina Lindemann, Oliver Hackmann, Sabit Delic, Natalie Schmidt, Guido Reifenberger, Markus J. Riemenschneider (2011) SOCS3 promoter methylation is mutually exclusive to EGFR amplification in gliomas and promotes glioma cell invasion. 2. Doktorandenkongress der Medical Research School Heinrich-Heine-Universität, Düsseldorf, 17. Juni 2011

2. Carina Lindemann, Oliver Hackmann, Sabit Delic, Natalie Schmidt, Guido Reifenberger, Markus J. Riemenschneider (2010) SOCS3 inactivation by promotor hypermethylation - A potential mechanism in gliomas without EGFR overexpression? 55. Jahrestagung der Deutschen Gesellschaft für Neuropathologie und Neuroanatomie (DGNN) im Rahmen der Neurowoche 2010, Mannheim, 22.-25. September 2010